

“Human displacements from tropical cyclone Idai attributable to climate change”

Benedikt Mester ^{1 2}, Thomas Vogt ¹, Seth Bryant ^{2 3}, Christian Otto ¹, Katja Frieler ¹, and Jacob Schewe ¹

¹ Potsdam Institute for Climate Impact Research, Potsdam, Germany

² Institute of Environmental Science and Geography, University of Potsdam, Potsdam, Germany

³ GFZ German Research Centre for Geosciences, Potsdam, Germany

Correspondence: Benedikt Mester (benedikt.mester@pik-potsdam.de)

Abstract

Extreme weather events, such as tropical cyclones, often trigger population displacement. The frequency and intensity of tropical cyclones is affected by anthropogenic climate change. However, the effect of historical climate change on displacement risk has so far not been quantified. Here, we show how displacement can be partially attributed to climate change, using the example of the 2019 tropical cyclone Idai in Mozambique. We estimate the population exposed to high water levels following Idai’s landfall, using a combination of a 2D hydrodynamical storm surge model and a flood depth estimation algorithm to determine inland flood depths from remote sensing images, for factual (climate change) and counterfactual (no climate change) mean sea level and maximum wind speed conditions. Our main estimates indicate that climate change has increased displacement risk from this event by approximately 12,600 - 14,900 additional displaced persons, corresponding to about 2.7 to 3.2%. The effect of wind speed intensification is larger than that of sea level rise. Besides highlighting the significant effects on humanitarian conditions already imparted by climate change, our study provides a blueprint for event-based displacement attribution.

1 Introduction

Between 1980 and 2021, an average of 45 tropical cyclones (TCs) globally have been recorded per year (Guha-Sapir et al., 2022). TCs pose a set of societal risks to coastal communities around the world. While related monetary losses are high, with an average of US\$ 57.2 billion every year since 2008 (Guha-Sapir et al., 2022), TCs also displace an average of 9.3 million people every year, with this hazard being responsible for 43% of all weather-related displacements (IDMC, 2022). Such forced displacements are associated with human suffering, as well as substantial financial costs (e.g., for providing shelter or from loss of economic production) and often require international assistance for disaster relief funds and humanitarian response (Desai et al., 2021).

41 At the same time, global climate change is expected to alter TC characteristics, resulting in an
42 increase in overall TC intensity (maximum wind speed and precipitation) and hence in the
43 frequency of very intense TCs (category 4-5 on the Saffir-Simpson scale), fundamentally
44 because of an increase in potential intensity due to warmer sea surface temperatures (SST)
45 (Emanuel, 2005, 2013, 1987; Knutson et al., 2020). Sea level rise (SLR), also driven by global
46 warming, additionally compound coastal flood risk associated with TCs (e.g., Garner Andra J.
47 et al., 2017; Lin et al., 2012; Resio and Irish, 2016). Historic TC data records are short and
48 partially inconsistent, making it difficult to determine the degree of intensification over time,
49 despite observed changes in some basins, such as the South Indian Ocean (Knutson et al.,
50 2019; Kossin et al., 2013, 2007; Webster et al., 2005). Moreover, existing TC datasets often
51 focus on maximum wind speed, neglecting coastal and inland flooding which may be the
52 dominant hazards, e.g., as for Hurricane Katrina or Hurricane Harvey (Bloemendaal et al.,
53 2021). Paleo climate records (Lin et al., 2014; Nott and Hayne, 2001) and synthetic TC tracks
54 (Bloemendaal et al., 2022, 2020; Emanuel et al., 2006) can be used to extend TC
55 records. However, sediment availability is limited to a few coastal stretches and the statistical
56 resampling process incorporates only the average observed climatic conditions, respectively,
57 hampering the assessment of global climate change impacts over longer time periods
58 (Bloemendaal et al., 2020). Nonetheless, given that global mean surface air temperature and
59 sea level have already risen above pre-industrial conditions by about 1.1°C and 0.20 m,
60 respectively (Gulev et al., 2021), it is likely that recent TC landfalls have caused more severe
61 societal impacts than would be expected without climate change. A probabilistic attribution
62 addressing this topic is limited by the shortness of TC records (Trenberth et al., 2015), and
63 may be additionally affected by multi-decadal variability (e.g., the Atlantic Multidecadal
64 Oscillation) or interannual climate variability (e.g., the El Niño–Southern Oscillation) (Patricola
65 and Wehner, 2018). As a consequence, the portion of TC-induced human displacements
66 attributable to climate change has so far not been quantified.

67
68 In this study, we address this research gap for the particular case of displacement triggered
69 by TC Idai in 2019. We examine the floods in central Mozambique associated with TC Idai,
70 considered to be “one of the Southern Hemisphere’s most devastating storms on record”
71 (Warren, 2019). On the 14th of March, Idai made landfall near the densely populated port city
72 of Beira, inhabited by more than 530,000 people (Figure 1). Alongside strong winds (maximum
73 1-min sustained winds of 180 km/h) and extensive inland flooding caused by heavy rainfall,
74 the cyclone also created a storm surge of up to 4.4 m, leading to coastal flooding centered at
75 the port city of Beira (Probst and Annunziato, 2019). In Mozambique alone, TC Idai claimed
76 the lives of more than 600 people, and caused 478,000 internal displacements, as well as
77 widespread structural damage totaling more than US\$ 2.1 billion (Guha-Sapir et al., 2022;
78 IDMC, 2022).

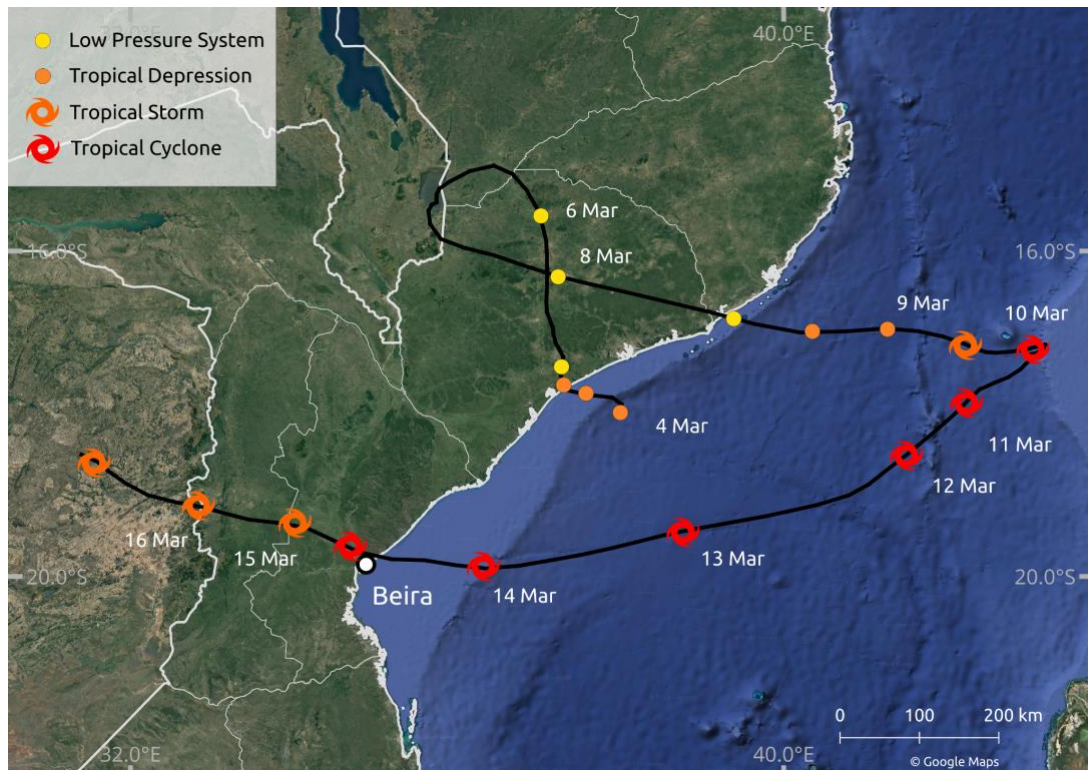
79
80 Here, we investigate how the coastal flooding would have manifested in a counterfactual world
81 without climate change, and consequently, how many of the observed human displacements
82 from TC Idai can be linked to climate change. For the attribution of the impacts we follow the
83 storyline approach introduced by Shepherd (Shepherd, 2016). To this end, we account for two
84 known mechanisms through which global climate change could have affected coastal flood
85 hazard: SLR and amplification of storm intensity. Storm track and size are not changed, even
86 though both parameters are subject to the effects of climate change (Knutson et al., 2020,
87 2019). We first estimate the influence of climate change on sea level and TC intensity in the
88 South Indian Ocean. We employ a high-resolution hydrodynamic flood model to simulate TC

89 Idai’s peak coastal flood extent and depth, both under historical conditions and under
90 counterfactual conditions with lower sea levels and lower maximum wind speed,
91 corresponding to a world without climate change. We additionally use satellite imagery to
92 account for inland (fluvial and pluvial) flooding, and estimate the total number of people
93 affected by flooding. We then model the number of displacements based on flood depth-
94 specific vulnerability factors, and estimate the fraction of displacements that can be attributed
95 to climate change by comparing results under factual vs. counterfactual conditions.

96
97 We use an estimate of SLR that attempts to separate natural variability in ice sheet and glacier
98 mass balance and retain only the long-term trend induced by global warming (Strauss et al.,
99 2021). Beyond this, however, our analysis is indifferent to whether the trends in sea level and
100 TC intensity are anthropogenic or not. This is in line with the definition of *impact attribution* put
101 forward by the Intergovernmental Panel on Climate Change (IPCC), where “changes in
102 natural, human, or managed systems are attributed to [a] change in [a] climate-related system”
103 (O’Neill et al., 2022). Such a question can be separated from the *climate attribution* question
104 of whether the change in the climate-related system - here, sea level and TCs - is due to
105 anthropogenic forcing. This separation allows us to focus on the link between climate change
106 and displacement despite remaining uncertainty about the exact anthropogenic contribution.
107 We will return to this issue in the discussion.

108
109 This study aims to attribute coastal-flood induced human displacements from TC Idai to
110 historic climate change, using a quantitative modeling approach. It addresses the need for
111 insights on the human impacts of climate change globally, and in particular in countries like
112 Mozambique that suffer from a combination of high exposure to climate-related hazards - in
113 this case, TCs - and high socio-economic vulnerability. Moreover, Mozambique, like many
114 other countries, is characterized by limited availability of in-situ observational data and a lack
115 of calibrated, local-scale inundation models. We use remote-sensing data and a globally
116 applicable modeling framework to characterize flood exposure during TC Idai; reported
117 displacement data is retrieved from the Global Internal Displacement Database (GIDD). Our
118 approach is thus transferable to other cases in virtually all relevant countries.

119
120
121
122
123
124
125



126
127
128
129
130
131
132

Figure 1: Trajectory of tropical cyclone Idai over the South Indian Ocean. Trajectory data is based on the IBTrACS database (Knapp et al., 2010). Mozambican administrative boundaries (GADM, 2018) in white; satellite image background by © Google Maps (Google Maps (a), 2022). Dates and tropical cyclone status adopted from ReliefWeb (ReliefWeb, 2019a).

133 2 Methods

134 2.1 Counterfactuals

135 Constructing counterfactuals for sea level and TC intensity requires estimating the effect of
136 historical climate change on these quantities. Total global mean sea level has risen by
137 approximately 23 cm since the turn of the 20th century (Church and White, 2011); at a rate
138 that has increased over time (Dangendorf Sönke et al., 2017). According to the IPCC, it is very
139 likely that the rate of global mean SLR was 1.5 (1.1 to 1.9) mm yr⁻¹ between 1902 and 2010,
140 and 3.6 (3.1 to 4.1) mm yr⁻¹ between 2006 and 2015 (Gulev et al., 2021). Nonetheless,
141 regional changes in sea level may differ substantially from the global average due to shifting
142 surface winds, the differential expansion of warming ocean water, and the addition of melting
143 ice, which can alter the ocean circulation (Fox-Kemper et al., 2021). Additionally, increases in
144 the amount of water stored on land (due to construction of dams and reservoirs), as well as
145 land subsidence, have also affected total sea level, with their relative effects varying
146 geographically (Church et al., 2004; Strauss et al., 2021).

147
148
149

Long-term in-situ observational records of SLR are scarce in the Indian Ocean (Han et al., 2010), hampering a precise detection of changes in sea level. For example, no active tide

150 gauge stations can be found on the coast of Beira (Beal et al., 2019), with the nearest station
151 located in Inhambane, Mozambique, 448 km south of Beira. However, regional historical SLR
152 rates for Mozambique, derived from satellite imagery or models, are close to global mean
153 estimates. IPCC rates of change in sea surface height (geocentric sea level) derived from
154 satellite altimetry show regional SLR off the coast of Mozambique at around 4.0 mm yr⁻¹ for
155 the period 1993–2012 (Church et al., 2013). Climate-induced SLR at the South-Eastern
156 African coastline (1993 - 2015) is estimated at ~3.5 mm yr⁻¹ using a coastal-length weighted
157 approach (Nicholls et al., 2021). Reconstructed sea level fields using global tide gauge data
158 suggests global-averaged SLR at 1.8 ± 0.3 mm yr⁻¹ over the 1950-2000 period, with regional
159 SLR off the coast of Mozambique at around 1.5 mm yr⁻¹ (Church et al., 2004). Han and
160 colleagues (Han et al., 2010) estimate regional Mozambican SLR at approximately 1.2 mm
161 yr⁻¹ between 1961-2008.

162
163 Given that these regional estimates are close to the global mean estimate by the IPCC, we
164 assume that total SLR near Beira is the same as the global mean, a comparable approach as
165 by Irish and colleagues (Irish et al., 2014). In order to exclude trends induced by natural
166 variability, particularly in sea level contributions from glaciers and ice sheets, we use estimates
167 of global mean sea level rise attributable to anthropogenic climate change for 1900–2012 from
168 Strauss and colleagues (Strauss et al., 2021). Their ensemble estimate is 6.6 to 17.1 cm,
169 which we use to define counterfactual sea level parameters for the coastal flood model. This
170 also implies assuming no substantial local effects of land subsidence and human-induced
171 changes in land water storage through reservoir construction and groundwater extraction that
172 would confound comparison with the global estimates. This is hard to verify, but can be
173 motivated by findings that city subsidence occurs only in a small fraction of the world's coasts
174 (Nicholls et al., 2021).

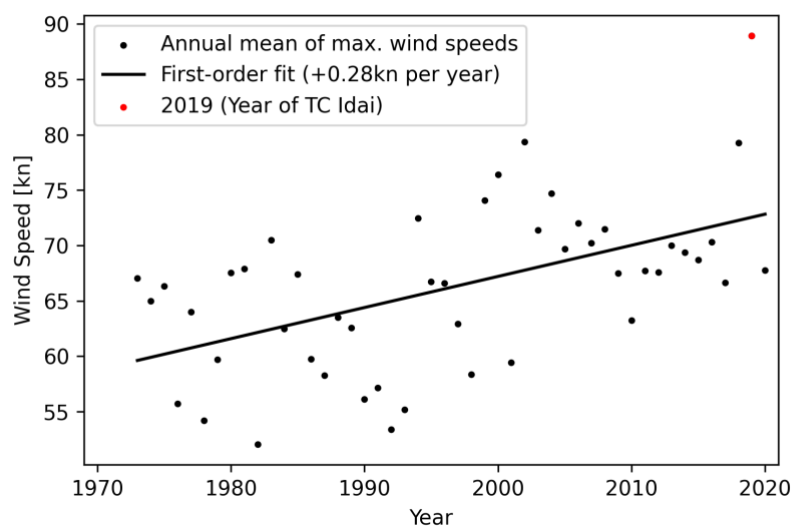
175
176 Tropical cyclones are projected to become more intense with rising temperatures (Knutson et
177 al., 2015), which is in line with the theoretical understanding of the potential intensity theory
178 (Emanuel, 1987). Observed TC wind speed data in the South Indian Ocean basin shows that
179 the maximum 10-minute sustained wind speed has been increasing by about 0.3 kn (0.15 m
180 s⁻¹) per year on average, over the period 1973-2019 (Figure 2). Prior to 1973, the rate of
181 increase was likely smaller, though observational data is lacking. We make a conservative
182 assumption corresponding to 50 years of increase at a rate of 0.2 kn (0.1 m s⁻¹) per year,
183 resulting in a total difference in maximum wind speed of approximately 10 kn (5.1 m s⁻¹). For
184 the case of TC Idai with maximum observed 10-minute sustained wind speeds of 105 kn (54
185 m s⁻¹), this corresponds to a 10% reduction in maximum wind speed by removing climate
186 change, which we adopt as a plausible assumption for counterfactual TC intensity.

187
188
189
190 This value is in line with the remote sensing-based estimates provided in Kossin et al. (2013),
191 who find that lifetime maximum TC intensities in the SIO have increased by about 4.6 m/s over
192 the period 1982-2009 (1.7 m/s per decade), which corresponds to 8.5% of TC Idai's maximum
193 intensity. If this rate of increase is linearly extrapolated to 2019, it results in an increase of
194 about 6.3 m/s (11.6%). Since the rate of increase has likely risen along with surface warming,
195 and since our period of reference extends back to 1973 rather than 1982, a value of 12% might
196 be a safer assumption for comparing the results of Kossin et al. (2013) with our own estimate.

197 To quantify the effect of uncertainty in the estimate of TC intensity change, we conduct two
198 sensitivity experiments, with counterfactual intensity lower than factual by 8.5% and 12%,
199 respectively, reflecting the SOI estimate of Kossin et al (2013) both directly and when
200 extrapolated for comparability with our own estimate.

201
202 We note that lower rates of change have been found in climate model-based studies. Knutson
203 et al. (2020) find a 6% increase in maximum intensity of SIO TCs per 2°C global mean surface
204 warming. When applied to the historical increase in global mean surface temperatures of
205 1.1°C, this would yield an increase of 3.3%. While these climate model estimates are important
206 both for assessing future changes and for understanding the underlying mechanisms of
207 observed trends, the remote-sensing based trend estimates are more relevant for informing
208 the construction of the counterfactual in our study.

209



210

211 Figure 2: Annual means of maximum TC wind speeds in the South Indian Ocean (maximum
212 10-minute sustained wind speeds). Linear trend over the period 1973-2020; data from
213 IBTrACS database (Knapp et al., 2010).

214 2.2 Coastal Flood Modeling

215 The storm surge flood simulations are generated using the open-source geophysical flow
216 solver GeoClaw (Mandli and Dawson, 2014). GeoClaw uses an efficient adaptive mesh
217 refinement to model wind- and pressure-induced wave dynamics in the 2-dimensional depth-
218 averaged shallow water equations. The input data includes TC tracks, astronomical tides, and
219 topographical raster data (see below) and GeoClaw provides outputs in the form of gridded
220 maps of maximum flood heights as well as the temporal dynamics of storm surge at virtual
221 tide gauge locations. We configure GeoClaw to limit the automatic mesh refinement to a
222 spatial resolution of between 1 and 8 arc-seconds (approximately 30 and 240 m) inside of
223 Idai’s landfall area and to between 100 and 900 arc-seconds (approximately 3 and 27 km) in
224 the open ocean.

225

226 As the factual input for GeoClaw, the TC track data from IBTrACS (Knapp et al., 2010)
227 provided by the WMO Regional Specialised Meteorological Center at La Reunion (operated
228 by MeteoFrance) is used. For the counterfactual scenarios with modified TC intensity, we
229 multiply all wind speed values along the track by a scalar factor of 0.9 (for a decrease of 10%
230 in intensity). The central pressure at each track position is increased by 0.1 times the
231 difference between central pressure and environmental pressure.

232
233 From the wind speed, pressure, and radius information provided along the TC track, GeoClaw
234 derives surface wind speeds and air pressure at arbitrary locations in space and time using a
235 radially symmetric wind profile (Holland, 1980) combined with the influence from the storm's
236 translational speed.

237
238 GeoClaw does not incorporate any tidal dynamics, nor meteorological forcings apart from the
239 TC wind and pressure fields mentioned above. To account for the influence of astronomical
240 tides, we configure GeoClaw to use an initial sea level according to gridded satellite altimetry
241 for 2019 (CMEMS, 2021), optionally enhanced by the minimum, mean, or maximum simulated
242 astronomical tides in the region of landfall according to the FES2014 global ocean tide atlas
243 (Lyard et al., 2021). For the counterfactual sea level scenarios, the amount of sea level rise
244 specified in the scenario description (between 6.5 and 17.0 cm) is subtracted from the initial
245 sea level.

246
247 The topographical input for GeoClaw is taken from digital elevation models (DEMs). We use
248 a combination of CoastalDEM 2.1 (Kulp and Strauss, 2021, 2018) in coastal areas, SRTM 15+
249 V2.3 (Tozer et al., 2019) over the open ocean and Multi-Error-Removed Improved-Terrain
250 (MERIT) DEM (Yamazaki et al., 2019) everywhere else. All datasets are converted to the
251 same geoidal vertical datum (EGM96) at a spatial resolution of 9 arc-seconds (approximately
252 300 m). This resolution is the highest resolution where we were able to obtain numerically
253 stable results from GeoClaw. We note that no harmonization has been applied to make up for
254 disagreements between the different DEM products so that the transition from CoastalDEM
255 topography to SRTM 15+ bathymetry can be steep.

256
257 Due to a lack of tide gauges or suitable observed flood extent in Mozambique, it is not possible
258 to validate the performance of GeoClaw for TC Idai in the factual model runs. However, we
259 compare the water levels at a virtual tide gauge station off the coast of Beira, where the highest
260 impacts from TC Idai have been reported, with simulated water levels from the Global Tide
261 and Surge Model (GTSM) (Dullaart et al., 2021; Muis et al., 2020), and find the best agreement
262 of maximum surge heights for the GeoClaw run with the maximum astronomical tide
263 assumption, closely followed by the run assuming the monthly mean sea level (no tidal
264 adjustment) (Supplementary Figure S1).

265 2.3 Inland Flood Depth Estimation

266 Gridded depth maximums for the flood event (Supplementary Figure S2) is calculated using
267 the Rolling HAND Inundation Corrected Depth Estimator (RICorDE) tool (Bryant et al., 2022)
268 supplied with terrain data from the MERIT DEM project, permanent surface water data from
269 the Joint Research Centre (JRC) Global Surface Water project (Pekel et al., 2016), and flood
270 extents from the FloodScan product (Atmospheric and Environmental Research & African Risk

271 Capacity, 2022). MERIT DEM provides a roughly 90 m resolution global layer derived from
272 multiple space-based sensors to minimize elevation errors. The maximum water extent layer
273 from JRC's Global Surface Water project provides a roughly 30 m resolution global layer of
274 locations detected as inundated on Landsat imagery (Wulder et al., 2016) from 1984-2019
275 (Pekel et al., 2016). Observed flood extents for TC Idai are obtained from Atmospheric and
276 Environmental Research & African Risk Capacity's accumulated 2-tier standard flood extent
277 depiction FloodScan product from 2019-03-01 to 2019-03-31 using the MERIT DEM
278 resolution. Originally developed for applications in Africa, this FloodScan algorithm relies on
279 satellite based low-resolution passive microwave data and was designed to capture national-
280 scale events. To accomplish this, the algorithm minimizes false-positives, making the
281 algorithm more prone to false-negatives and less sensitive to events with smaller spatial extent
282 and urban floods (Galantowicz and Picton, 2021). All data layers are re-projected to 90 m
283 resolution geodetic coordinates prior to the RICorDE computation.

284
285 RICorDE is a tool developed in pyQGIS for post-event analysis of fluvial flood events using
286 inundation masks derived from space-based observations. RICorDE first generates a Height
287 Above Nearest Drainage (HAND) grid followed by an inundation correction phase and a water
288 surface level (WSL) calculation phase. As part of pre-processing, the HAND grid is obtained
289 using WhiteboxTools' ElevationAboveStream (Lindsay, 2014) from the permanent surface
290 water layer and the DEM. In the first phase of RICorDE, the observed flood extents are
291 hydraulically corrected to account for under-predictions using the permanent surface water
292 layer and over-predictions using a HAND-derived inundation representing the upper quartile
293 of possible flooding extents. In the second phase, HAND values sampled from the inundation
294 shoreline are used to produce an interpolated WSL grid using WhiteboxTools' CostAllocation
295 algorithm (Lindsay, 2014). Finally, gridded water depths are obtained from this WSL grid
296 through subtraction with the DEM. RICorDE is explained in detail in the tool publication (Bryant
297 et al., 2022) and the source code can be accessed online
298 (https://github.com/ceflect/RICorDE_pub).

299
300 The slower, more complex RICorDE algorithm has been shown to produce more accurate
301 depths maps for two fluvial flood events in Canada when compared to faster, more disaster
302 response-focused solutions like the Floodwater Depth Estimation Tool (FwDET) (Bryant et al.,
303 2022; Cohen et al., 2018). While no data is available to validate the performance of the depths
304 estimate for TC Idai, visual inspection suggests results are less accurate in areas with higher
305 elevation (>20 m), especially where drainageways are of comparable width to the resolution
306 of the JRC water extent layer. These false negatives in the JRC layer propagate as positive
307 bias in the HAND routine, which leads to higher elevation water surface predictions and similar
308 positive bias in the depth values (see white arrow in Figure S3a).

309 2.4 Combined Flood Depth Product

310 The inland flood depth estimates from RICorDE are resampled from 3 arcsec to 9 arcsec,
311 using the average resampling method (Rasterio library for Python), to match the resolution of
312 the GeoClaw output. All flood depths are rounded to the nearest decimeter, their outline is
313 cropped to the area of interest, and the final factual flood depth in each grid cell (shown in
314 Figure 3a) is determined as the maximum of both products. This accounts for both potentially

315 partly obscured satellite imagery by clouds and potential underestimation by the numerical
316 model.

317

$$318 \quad d_0 = \max (d_{c,0} , d_r) \quad (1)$$

319

320 with d_0 referring to the factual flood depth, and indices c and r referring to the coastal flood
321 model (GeoClaw) and to the remote sensing data translated into flood depth using RICorDE,
322 respectively. To derive the counterfactual flood depth d_{cf} , we subtract the difference between
323 modeled factual and counterfactual coastal flood depths from the combined factual flood
324 depth:

325

$$326 \quad d_{cf} = d_0 - (d_{c,0} - d_{c,cf}) \quad (2)$$

327

328 2.5 Displacement

329 We use displacement data from the publicly accessible GIDD, maintained by the *Internal*
330 *Displacement Monitoring Centre* (IDMC, 2022). IDMC follows the definition of displacement
331 provided in the Guiding Principles on Internal Displacement (OCHA, 2004), which states that
332 “[i]nternally displaced persons are persons or groups of persons who have been forced or
333 obliged to flee or to leave their homes or places of habitual residence, ... and who have not
334 crossed an internationally recognized State border”. This definition covers permanent
335 displacement, temporary displacement, and pre-emptive evacuations (Gemenne, 2011), all
336 summarized as “displacements” within our study. No granular information is available in GIDD
337 on the type of displacement. Displacement numbers are based on multiple secondary sources,
338 such as IOM, OCHA, or - in the case of TC Idai - the Mozambique National Institute of Disaster
339 Management. The TC Idai event is categorized as a “storm” event, however, no information is
340 given on how many of the displacements were caused respectively by flooding, strong winds,
341 or a combination of both. Because of the extensive flooding observed in the wake of Idai’s
342 landfall and humanitarian reports often focused on flooding (ReliefWeb, 2019a), we assume
343 in our main analysis that all displacements are caused by flooding (either coastal or inland).
344 We assume that people exposed to flood levels greater or equal than 100 cm are affected by
345 the flooding and thus prone to displacement, following previous studies (Custer and Nishijima,
346 2015; Kam et al., 2021). However, we also test the sensitivity of our results to this threshold
347 choice by evaluating alternative water level thresholds of 10 cm and 50 cm. Our modeling
348 approach assumes an artificially deterministic link between the TC hazard and displacement,
349 which is adequate in the context of the factual-counterfactual approach where only one
350 parameter - storm surge hazard - is modified while everything else, including vulnerability, is
351 held constant. In general, the relationship between climatic events, pre-existing socio-
352 economic conditions, and displacement is complex and only partially understood (Cattaneo et
353 al., 2019; UK Government Office for Science, 2011). In other words, our study addresses the
354 question of how many displacements might have occurred in a different climate but with the
355 same vulnerability as observed; it does not address the question of how this vulnerability came
356 about.

357

358 We first determine the flood extent with depths greater than the selected water level threshold
359 and overlay it with population data to estimate the number of people affected. We use gridded

360 population data from GHS-POP (Schiavina et al., 2019) for the year 2015, on 9 arcsec
361 resolution. Population growth in Mozambique was 1.12 % between 2015 and 2019 (The World
362 Bank, 2022); we hence multiply all population grid cells with this factor, assuming a spatially
363 equal population growth.

364

365 We then calculate the ratio between the number of observed displacements, and the number
366 of affected people from the factual flood estimate. This ratio, which may be thought of as an
367 event-specific displacement vulnerability factor, is different for every tide assumption,
368 reflecting the uncertainty about the actual flood extent and depth. We compute for every
369 impact level threshold i and tide assumption h a displacement vulnerability factor $v_{i,h}$ by
370 dividing the number of observed displacements D_o by the total number of affected people of
371 the factual scenario $A_{i,h,o}$:

372

$$373 \quad v_{i,h} = \frac{D_o}{A_{i,h,o}} \quad (3)$$

374

375 Multiplying the specific displacement vulnerabilities with the counterfactual numbers of
376 affected people, we derive the number of people at risk of displacement in a world without
377 climate change. This means that the difference between factual and counterfactual
378 displacement estimates comes only from differences in the flood hazard, while exposure and
379 vulnerability factors are held fixed. We achieve this by multiplying $v_{i,t}$ with the number of
380 affected people of the counterfactuals $A_{i,h,cf}$, and estimate the expected number of
381 displacements for each counterfactual scenario $D_{i,h,cf}$:

382

$$383 \quad D_{i,h,cf} = v_{i,h} * A_{i,h,cf} \quad (4)$$

384

385 We point out that the use of predefined flood thresholds implies the assumption that at a given
386 flood depth, the risk of severe damages to, or even destruction of, residential buildings and
387 other infrastructure typically becomes so large that people may be forced to flee. The number
388 of people that actually become displaced then depends on additional physical, political and
389 socio-economic factors, which may vary between local contexts and are not generally known.
390 Their aggregate effect is reflected in the specific vulnerability factor $v_{i,h}$. In other words, the
391 link between flood hazard and displacement is “soft” in the sense that it is mediated by the
392 local vulnerability. An alternative assumption would be that there is an (event-specific) flood-
393 depth threshold below which there is no displacement, and above which people become
394 displaced regardless; that is, a “hard” link between flood hazard and displacement. In this
395 case, the flood-depth threshold could be derived directly from the data, as the depth level at
396 which the calculated number of affected people equals the reported number of displacements.
397 When we sum up the affected people per 10 cm flood depth increment for TC Idai, we obtain
398 a threshold of about 400 cm (similar for all tide assumptions; Supplementary Table S1), for
399 which the modeled number of affected people approximately equals the number of observed
400 displacements. This value is very high in comparison with the thresholds cited further above,
401 and we believe it is implausible for displacement to occur only in locations inundated by 4
402 meters or more. This exercise therefore lends further justification for the “soft link” approach.

403

404

405 Even though disaster reports for TC Idai suggest flooding to be the main driver of
406 displacement, high wind speeds may have locally intensified the impact of TC Idai (Figure S4)

407 and be partially responsible for the observed displacements. We conduct an additional
408 analysis where we assume that people affected by either flooding or wind (or both) were at
409 risk of displacement with an equal vulnerability factor. We use a wind speed threshold of 96
410 kn (50 m s^{-1}) for population exposure (Geiger et al., 2018), corresponding to the Saffir–
411 Simpson scale classification 3 (major hurricane). The resulting wind field is overlaid with
412 gridded population data to compute the number of affected people, excluding those who are
413 already affected by flooding.

414 3 Results

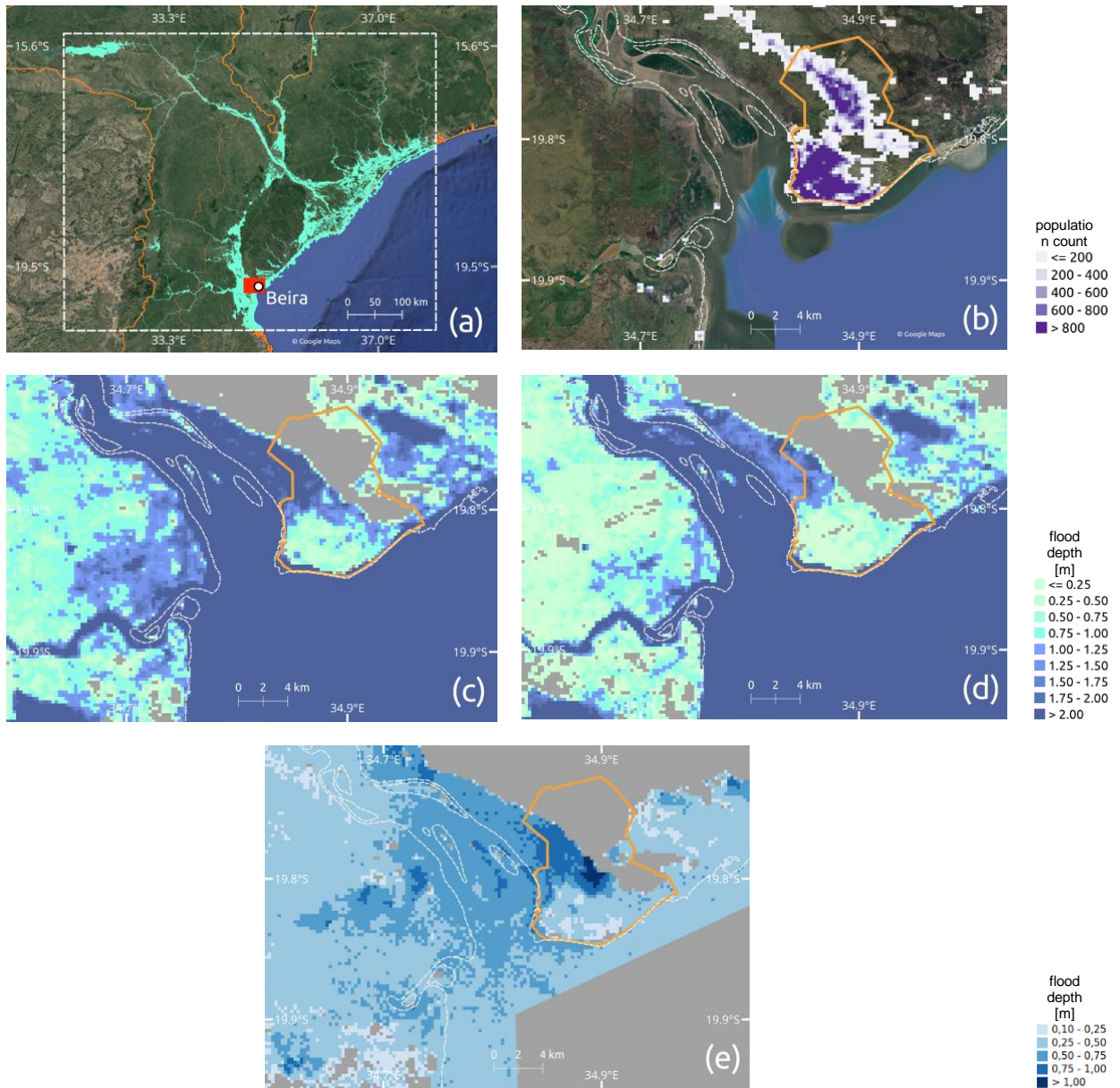
415 3.1 Simulated flooding

416 We calculate storm surge flood extent and depth for the factual (driven with observed wind
417 speeds and sea levels) and counterfactual (reduced wind speeds and sea level) scenarios.
418 The difference between factual and counterfactual flooding (maximum tide, 10.5 cm SLR, 10%
419 TC intensification) is illustrated in the densely populated area of Beira (Figure 3b), the city
420 where TC Idai made landfall and destroyed 90% of all houses according to some disaster
421 reports (ReliefWeb, 2019b). Beira consists of two major population centers, of which the
422 southern one is close to the seaside and exhibits a higher population count.

423
424 Both factual and counterfactual flood extent covers the southern, highly populated part of Beira
425 (Figure 3c and 3d). The northern parts of the city are only marginally affected. Flood extents
426 are also similar between factual and counterfactual simulations in the areas east of Beira and
427 around the inflow of the Buzi River, located on the opposite side of the bay. Only a few isolated
428 locations no longer experience flooding after removing the effects of climate change.

429
430 In contrast, differences in simulated flood depth are more pronounced (Figure 3e).
431 Counterfactual flood depths are up to 80 cm lower than factual flood depth in some parts of
432 the southern city center. The highest difference in flood depth, of up to 140 cm, is found
433 between the northern and southern population centers of Beira. Flood depth differences
434 outside of Beira are rather low, however, Figure 3c and 3d show that absolute flood depths
435 drop below the critical flood depth of 100 cm over great parts around the west bank of the
436 Pungwe River inflow.

437
438
439
440
441
443
444



445
446
447
448
449
450
451
452
453
454
455
456

Figure 3: Simulated flood extent for Mozambique; population distribution and inundation levels for the greater area of Beira. (a) Combined factual estimate of inland and coastal flooding (binary; flood/no-flood). White dashed box shows the area of interest in which flood exposure is computed. Red rectangle shows the extent of the section displayed in panel (b) - (e). (b) Population distribution for the greater area of Beira. Flood extent and levels for (c) the factual scenario (max. tide), and (d) the “counterfactual TC intensity + sea level rise (10.5 cm) - max. tide” scenario. Flood depth difference between (c) and (d) is displayed in (e). City neighborhoods of Beira (HDX, 2019) are indicated by orange lines and shoreline (Wessel and Smith, 1996) is represented by dashed white lines in (b) - (e); satellite image background by © Google Maps (Google Maps (b), 2022) in (a) and (b).

457 3.2 Displacement

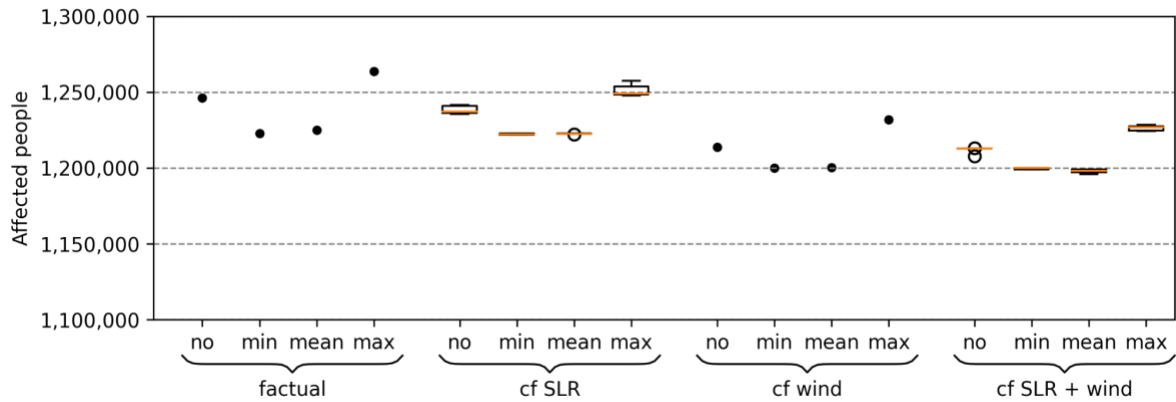
458 In the next step, we investigate how the factual and counterfactual flood estimates translate
459 into population at risk of displacement for the whole of Mozambique. We compare factual and

460 counterfactual affected people/displacements and compute the absolute relative change
461 based on the counterfactual results, representing the increase in impact due to climate
462 change. Our analysis shows that the intensification of TC wind speeds leads to an increase in
463 flood affected people and, consequently, in displacements by up to 2.7%, while
464 counterfactuals regarding the sea level lead to only small changes by up to 1.3 % (Figure 4,
465 Table 1 and Table S2). A combination of both counterfactuals only slightly exceeds the range
466 (increase by up to 3.2% for the maximum tide assumption) as in contrast when considering
467 the TC intensification alone. Despite the large uncertainty regarding SLR since 1900, the
468 difference in the number of people affected (or displaced) is rather marginal; being less than
469 1% increase between the largest and the smallest SLR estimate for the “cf SLR” simulations.
470 Our results highlight that the tide assumption plays a major role. The minimum and mean tide
471 lead to marginal changes in affected/displaced people, in contrast to the maximum
472 astronomical tide and monthly mean sea level from satellite altimetry (no tide), which show for
473 the “cf SLR + wind” simulations a median change in 3.0% (maximum change in 3.2%) and
474 2.7% (3.2%), respectively. Given the high number of affected people, already small changes
475 in the counterfactual scenarios lead to high changes in absolute numbers. The coupled effect
476 of higher wind speeds and higher sea level increases the number of affected people and
477 displacements by up to 39,300 and 14,900 (maximum tide) and 38,100 and 14,600 (monthly
478 mean), respectively. Results regarding impact flood levels of 10 cm and 50 cm are displayed
479 in Table 1 and the supplementary material (Figure S5 and S6), showing even higher changes
480 for the counterfactual scenarios of up to 56,500 displacements (13.4% increase).

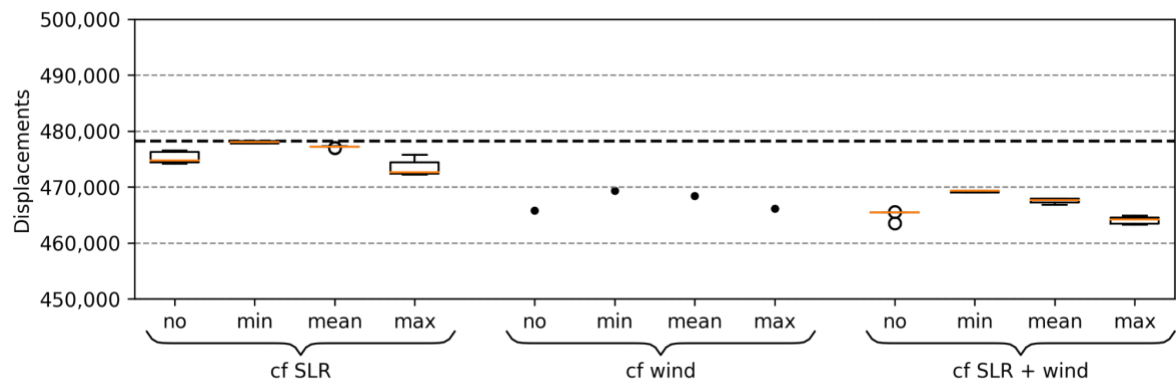
481
482 Besides our central TC intensification assumption of 10%, we also examine two alternative
483 assumptions of 8.5% and 12% intensification, respectively, for the “max” tide (Figure 5). The
484 spread among the intensification scenarios is rather small, with median relative changes
485 varying between 2.9% and 3.7%. This translates to median estimates of 35,300 and 44,600
486 affected people, or 13,400 and 16,900 displacements, respectively (Table 1 and Table S2). In
487 contrast, the difference between the highest (4.0%) and lowest values (2.2%) is larger. In
488 absolute terms, this means a range of between approximately 27,400 and 48,200 affected
489 people, or 10,400 and 18,200 displacements.

490
491 We assume that high wind speed caused only a marginal fraction of displacements, following
492 disaster reports, media coverage and experience from other events; as an extreme example,
493 wind by Hurricane Sandy caused less than 0.01% of the overall damage (Strauss et al., 2021).
494 Nonetheless, in an additional sensitivity analysis, we also account for the number of people
495 affected by high TC wind speeds of 50 m s^{-1} or above (Sect. Methods). Our analysis reveals
496 that the number of people affected not by flooding (maximum tide assumption, 100 cm impact
497 threshold) but by high wind speeds ranges between 340,900 to 360,600 in the factual
498 simulation. In the counterfactual, even the maximum wind speed attained in any grid cell
499 outside the flooded area drops from 51.5 m s^{-1} to 46.3 m s^{-1} , i.e. below the above-mentioned
500 threshold; thus, no people are counted as affected. Assuming the same vulnerability factor
501 for displacement due to high wind speed as due to flooding yields 103,700 to 112,100
502 displacements, or 21.7 to 23.4% of the total displacement, attributable to climate change.

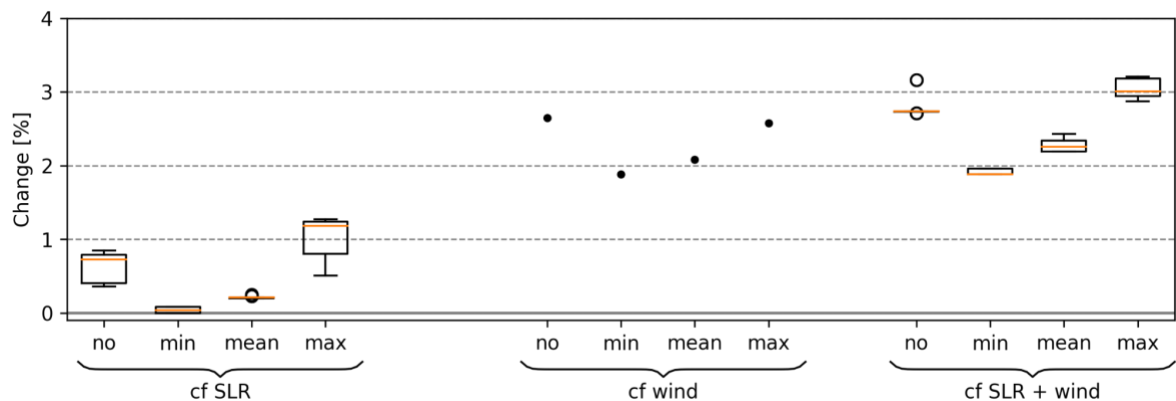
503
504
505
506



507



508



509

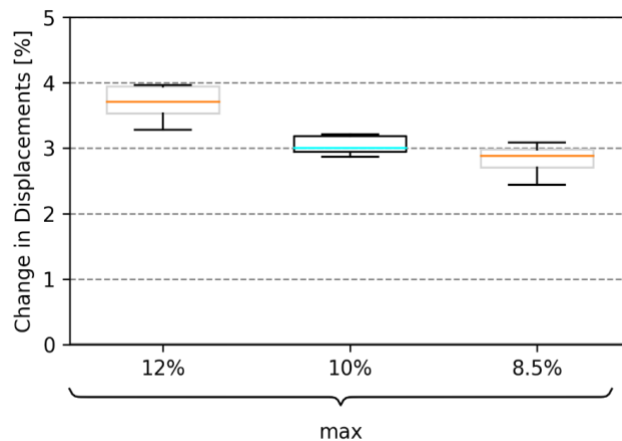
510 **Figure 4: Simulated affected people (top), displacements (middle) and percentage**
 511 **change (bottom) for the 100 cm impact threshold.** The percentage change compares
 512 factual and counterfactual displacements, and represents the absolute relative change based
 513 on the counterfactual results. Three counterfactual scenarios are shown: lower sea level (“cf
 514 SLR”), intensification (“cf wind”), and a combination of both (“cf SLR + wind”). Additionally,
 515 a variety of counterfactual sea levels as well as a set of astronomical tides is presented, covering
 516 minimum (“min”), mean (“mean”), and maximum (“max”) as well as monthly mean sea level
 517 from satellite altimetry (“no”). Bold dashed line in the middle panel shows the number of

518 observed displacements. Percentile changes in affected people and displacements are the
 519 same. The second quartile Q2 (median) of the box plot is shown in orange, “whiskers” are
 520 placed at $\pm 1.5 \cdot$ interquartile range (Q3-Q1).

521
 522 Table 1: Overview main results for modeled displacement impact. Min./Median/Max. are
 523 related to the SLR scenarios. Orange background of the first results row indicates the primary
 524 parameter estimate. Cells with gray background indicate the altered parameter in comparison
 525 with the primary estimate.
 526

Counterfactual	Flood Depth Threshold [cm]	Intensification [%]	Tide	Displacements Dif. Min.	Displacements Dif. Median	Displacements Dif. Max	Displacements Dif. Min. [%]	Displacements Dif. Median [%]	Displacements Dif. Max [%]
SLR + wind	100	10	max	13331	13958	14875	2.9	3.0	3.2
SLR + wind	100	10	no	12620	12740	14629	2.7	2.7	3.2
SLR + wind	100	10	min	8822	8822	9183	1.9	1.9	2.0
SLR + wind	100	10	mean	10235	10543	11353	2.2	2.3	2.4
SLR + wind	50	10	max	46695	49336	52275	10.8	11.5	12.3
SLR + wind	10	10	max	28557	32218	34456	6.4	7.2	7.8
SLR	100	10	max	2407	5584	5981	0.5	1.2	1.3
wind	100	10	max	-	12033	-	-	2.6	-
SLR + wind	100	8.5	max	10384	13354	14321	2.2	2.9	3.1
SLR + wind	100	12	max	14297	16870	18232	3.1	3.7	4.0

527



528

529 Figure 5: Percentage change in displacements between factual and counterfactual, for three
 530 different TC intensification assumptions. The percentage change compares factual and
 531 counterfactual displacements, and represents the absolute relative change based on the
 532 counterfactual results. The combined counterfactual scenario (“cf SLR + wind”) with 100 cm
 533 impact threshold and the maximum astronomical tide (“max”) is displayed. The central
 534 assumption of 10% intensification is highlighted with a cyan-colored median in the box plots.
 535 The second quartile Q2 (median) of the box plot is shown in orange/cyan, whiskers are placed
 536 at $\pm 1.5 \cdot$ interquartile range (Q3-Q1).

537 4 Discussion and conclusions

538 With more than one degree of global warming, most, if not all, extreme weather events now
 539 can be assumed to bear some imprint of climate change. By extension, this is also true for the
 540 humanitarian crises induced by catastrophic storms, floods, or droughts. However, while
 541 economic damages from climate change have been attributed both in case studies and global

542 studies (Frame et al., 2020b, 2020a; Sauer et al., 2021; Strauss et al., 2021), little is known
543 about the extent to which climate change has already exacerbated human displacement. Our
544 modeling study of TC Idai suggests that climate change may have induced between 12,600
545 (2.7%; lowest estimate under the no tide assumption) and 14,900 (3.2%; highest estimate
546 under the maximum tide assumption) additional displacements from this one event. This is
547 primarily due to the intensification of TC wind speed inducing a more powerful storm surge;
548 and to a lesser extent due to sea level rise providing a higher baseline for the storm surge.
549 We also show that the sensitivity of the results to the choice of TC intensification is
550 approximately in the same range as for the tide assumption.

551
552 Our results likely underestimate the full contribution of climate change to displacement
553 associated with TC Idai, because we solely addressed the effect of climate change on coastal
554 flooding, neglecting changes in inland flooding. Between March 3 and 17, heavy precipitation
555 between 200-400 mm was registered for Beira City and the region, with upstream sections of
556 the Pungwe River basin exposed to more than 600 mm (Probst and Annunziato, 2019). With
557 growing evidence that climate change not only affects precipitation intensity (Fowler et al.,
558 2021; Guerreiro et al., 2018; Scherrer et al., 2016) but also continental-scale changes in fluvial
559 flood discharge (Blöschl et al., 2019; Gudmundsson et al., 2021), it is likely that in a world
560 without climate change, the river flood magnitude would have been smaller, and even less
561 people would have been exposed than in our coastal-only counterfactual. Quantifying this
562 additional effect would require a river flood model capable of reproducing the observed flood
563 extent and associated inundation depths, and ideally coupled with a coastal flood model to
564 capture the interaction between river flood and storm surge. Even though globally-applicable
565 frameworks for compound flood hazard modeling are under construction, and have recently
566 been tested for TC Idai (Eilander et al., 2022), evaluations of fluvial flood models reveal
567 important shortcomings in data-scarce regions such as Mozambique (Bernhofen et al., 2018;
568 Mester et al., 2021). Quantifying the role of river flooding in TC-induced displacement thus is
569 a timely challenge.

570
571 The inland river flood estimates based on satellite imagery exhibit several limitations and
572 uncertainties. In the absence of validation data, it is difficult to quantify the uncertainty arising
573 from the inland flood depths estimation. These gridded values are highly sensitive to the input
574 layers, namely the DEM (MERIT), permanent surface water (JRC), and the satellite-based
575 observation of inundation extents (FloodScan). Especially uncertainties regarding the choice
576 of DEM, used for both the inland flood depth estimation and the coastal flood model, should
577 not be neglected (Hawker et al., 2018). Qualitatively, the performance seems poor in areas
578 with higher elevations (>20m). This could be attributable to challenges in representing the
579 topography at 90 m resolution and dense obstructions that scatter returning signals (Shen et
580 al., 2019).

581
582 Similarly, no suitable validation data for the coastal flood simulations is available. According
583 to the AER description, the used products “depict large scale, inland river flooding well but are
584 less likely to depict flooding in smaller floodplains and near coastlines”. We have hence opted
585 to not choose the AER product as the sole coastal flood hazard estimate nor as validation
586 dataset for the flood extent from our coastal flood model. A flood risk screening for Beira (van
587 Berchum et al., 2020) [showed that simulated flood extent for a 10-year rainfall event plus a
588 10-year coastal surge event covers most parts of the Central and Munhava city districts of
589 Beira \(South-Eastern city districts\). In contrast, the satellite imagery by AER shows only little](#)

590 flooding in this area, while it is assumed that flooding by TC Idai exceeded an average
591 recurrence interval of 10 years. For example, Emerton et al. (2020) show that GloFAS flood
592 forecasts indicated a 100% probability of exceeding the severe flood alert threshold (20-year
593 return period) for TC Idai at the Pungwe River (Emerton et al., 2020). Furthermore, newspaper
594 photographs (Bergensia, 2019) show flooding in the Area de Baixa part of Beira (Western
595 district of Beira), which was only partially flooded according to the satellite imagery. The AER
596 product thus likely underestimates flood extent, which may be explained by cloud
597 obscurement or failure in automatic flood detection due to, for example, flooding in densely
598 populated areas, or the satellite passing over some time after the peak flooding when water
599 levels have already receded.

600

601 Furthermore, the coastal flood modeling framework does not incorporate any astronomical
602 tidal dynamics. Because there are no tide gauge records available in the region, we were only
603 able to compare the model's surge heights to the state-of-the-art Global Tide and Surge Model
604 (GTSM). For the derived flood maps, there were no observational benchmarks available for
605 validation. Moreover, the model is not able to take the interaction of the coastal surge with
606 increased river discharge at the estuaries into account. In some cases, this interaction has
607 been shown to influence water levels in a nonlinear way, for example for the 2016 Louisiana
608 flood (Bilskie and Hagen, 2018). Another source of uncertainty is again the DEM, in particular
609 the transition from topographic to bathymetric data at the coast lines.

610

611 Additionally, our analysis may be sensitive to the choice of population dataset (Archila Bustos
612 et al., 2020; Leyk et al., 2019), which may lead to uncertainties regarding our estimated
613 exposure. No information is available regarding the spatial distribution of displacements within
614 GIDD; we assume that vulnerability to displacement is uniform across the affected area. The
615 total number of displacements is furthermore not specifically categorized by hazard type,
616 which reflects the multivariate (wind, rain and flood) compound characteristic of TCs hazards
617 (Zscheischler et al., 2020). However, this impedes the attribution of coastal flood-induced
618 displacements. Furthermore, the GIDD estimates include different forms of displacement,
619 such as forced displacement or pre-emptive evacuations, with the latter potentially accounting
620 for a substantial proportion (McAdam, 2022). This poses far-reaching implications for
621 displacement risk modeling, as evacuations may already be triggered by lower flood depths,
622 or by early warnings of an impending hazard, which may not materialize in the expected
623 manner, or may not cause the level of destruction that would lead to a corresponding
624 magnitude of forced displacement.

625

626 Our main analysis also assumed no direct effect of high wind speeds on displacement, lacking
627 clear evidence for substantial displacement due to high winds alone. Our additional sensitivity
628 analysis suggests that changing this assumption could increase the number of displacements
629 attributable to climate change considerably. Given this potentially large effect, and our limited
630 understanding of the relative roles of different drivers of displacement in general, the specific
631 vulnerability to displacement from different types of hazard should be the subject of future
632 studies. Moreover, assuming that displacement can occur already at inundation depths of less
633 than 100 cm also leads to higher estimates of climate change-attributable displacement,
634 according to our sensitivity analysis. We also tested if the flood depth threshold can be
635 estimated from the data by summing up the affected people per 10 cm flood depth increment
636 until equaling the number of observed displacements. This analysis yields an alternative flood
637 depth threshold of 400 cm, which we assess to be physically not reasonable in the context of

638 building structure in Mozambique. Again, a better understanding of vulnerability beyond hard
639 physical flood depth thresholds and empirically derived vulnerability factors will be critical to
640 refine risk assessments. Future work may produce a functional relationship between
641 displacement risk, contextual drivers, and physical flood properties, covering, for example,
642 depth, velocity, and duration.

643

644

645 We did not change storm track or size in our counterfactual simulations. While storm tracks
646 may be affected by climate change (Knutson et al., 2019), we assume that Beira has not
647 become more or less likely as a landfall site. Mean storm size is found to increase
648 systematically with the relative sea surface temperature (Chavas et al., 2016), although
649 numerical simulations suggest that projected median sizes remain nearly constant globally
650 (Knutson et al., 2015). Assuming increases in storm size due to climate change would again
651 result in higher estimates of attributable displacements in our analysis.

652 By design, in our attribution study, we assumed a fixed population distribution in both factual
653 and counterfactual simulations, as well as a fixed, empirically determined displacement
654 vulnerability factor, and only investigated changes in displacement risk following from changes
655 in the physical characteristics of TC Idai and its impacts. Assessments of future risks - or of
656 past impacts - should not only take into account the intensification of physical hazards, but
657 also changes in exposure (Kam et al., 2021); as well as potential changes in vulnerability due
658 to social, economic, or technological developments. For instance, TC-related displacements
659 depend not only on the damage to housing, but also on other factors such as government
660 responsiveness or poverty levels (Cissé et al., 2022).
661 Here, we have chosen a storyline approach for the impact attribution instead of a more
662 traditional probabilistic attribution approach (Philip et al., 2020; Titley et al., 2016), as for
663 instance previously employed to attribute heavy precipitation of Hurricane Harvey
664 (Oldenborgh et al., 2017) to climate change. One reason is that for Mozambique neither the
665 complete time series of rainfall nor the high station density required by a probabilistic approach
666 (van Oldenborgh et al., 2021) are available. Reanalysis products for precipitation could be
667 used as an alternative, however, their quality depends on geographic location, so the use of
668 multiple reanalysis and/or observation products is recommended (Angélil et al., 2016).
669 Nonetheless, a climate attribution approach focusing on changes in the probability or intensity
670 of TCs in the South Indian Ocean due to anthropogenic forcing (O'Neill et al., 2022) could
671 guide the construction of counterfactual scenarios of the storyline approach. Further, in
672 contrast to the probabilistic approach, the storyline approach allows us to investigate the
673 driving factors involved, as well as their plausibility (Shepherd et al., 2018).

674

675 Framing the risk of tropical cyclones in the context of climate change in an event-specific rather
676 than a probabilistic manner also allows us to assign absolute numbers of attributable
677 displacements, which raises risk awareness in a more tangible way. The responsibility for
678 managing and reducing displacement risk lies primarily at the national and provincial level, but
679 often local authorities, organizations, and communities respond to displacement disasters
680 (Hollinger and Sienkevych, 2019). Demonstrating quantitatively how climate change affects
681 the societal risks associated with natural hazards may play an important role in raising
682 awareness, with different types of stakeholders, to the changing nature of such risks. It may
683 also incentivize governments to step up their efforts both in terms of planning and investing
684 into adaptation measures, and rapidly mitigating greenhouse gas emissions. The storyline
685 approach is particularly suited for highlighting the risk-amplifying effects of climate change in

686 a tangible and accessible way, based on a well-known event in the recent past (van den Hurk
687 et al., 2023). Estimates of the costs of displacement additionally highlight the adverse
688 economic aspects of climate change (Desai et al., 2021); average costs have been put at \$310
689 per displaced person per year, though actual costs are heavily dependent on the country and
690 duration (days/weeks to years) (IDMC, 2019). Only 50.7% of the required Mozambique
691 Humanitarian Response Plan 2019 of US\$m 620.5 was funded, demonstrating that climate
692 change poses an additional burden to insufficiently equipped financial aid resources.
693 Anticipating the intensification of tropical cyclones under future global warming (Knutson et
694 al., 2020) calls for enhancing adaptation measures as well as disaster relief and humanitarian
695 aid. The IPCC AR6 projects an additional global increase in mean sea level and surface
696 temperature of 0.44 m / 1.2°C (SSP1-2.6) and 0.77 m / 4.0°C (SSP5-8.5), relative to a baseline
697 of 1995-2014, by the end of the 21st century (Fox-Kemper et al., 2021; Lee et al., 2021). Even
698 though these increases may vary between basins, an enhanced displacement risk due to Idai-
699 like TCs needs to be accounted for in the next decades, especially if future changes in
700 exposure due to population growth and urbanization are considered.

701
702 Our study expands the scope of extreme event impact attribution to include displacement as
703 a societal impact dimension. In general, due to the lack of calibrated regional models and
704 gauge stations, only few attribution studies (Luu et al., 2021; Takayabu et al., 2015) focus on
705 storms - or any extreme weather events, for that matter - in low-income countries. This not
706 only limits our understanding of climate change effects on extreme events from a global
707 perspective, but also biases geographically the amount of knowledge and information
708 available to inform risk management and adaptation strategies (Otto et al., 2020). Our impact
709 attribution is built on global-scale datasets and models, which could be employed in other
710 relevant locations. Despite the discussed limitations and uncertainties inherent to this
711 approach, displacements could be similarly attributed to climate change for other major TCs
712 that occurred in data- and model-scarce regions, such as Typhoon Haiyan (Philippines; 4.1
713 million displacements) or Cyclone Amphan (India and Bangladesh; combined 4.95 million
714 displacements) (IDMC, 2022) The continuing increase in spatial resolution of global-scale
715 products will eventually allow for more granular displacement risk assessments, which
716 regional authorities could incorporate in urban development plans, zoning regulations or
717 required building codes (IDMC, 2019). Mozambique, like many countries, is exposed not only
718 to TCs but also other climate-related hazards, such as droughts, and at the same time facing
719 socio-economic challenges, making it all the more important to understand and anticipate risks
720 in a changing climate. Our approach may hence be extended to large-n impact attribution,
721 using, for example, global counterfactual climate datasets (Mengel et al., 2021).

722 Code availability

723 The source code for this study is available from
724 https://github.com/BenediktMester/TC_Idai_attribution.
725

726 Data availability

727 Satellite imagery is used with the permission of Atmospheric and Environmental Research &
728 African Risk Capacity. Output of the flood depth algorithm, GeoClaw results, and TC Idai wind
729 speed files can be accessed at <https://zenodo.org/record/6907855> (Mester et al., 2022). GHS
730 gridded population data is available at [https://data.jrc.ec.europa.eu/dataset/jrc-ghsl-
731 ghs_pop_gpw4_globe_r2015a#dataaccess](https://data.jrc.ec.europa.eu/dataset/jrc-ghsl-ghs_pop_gpw4_globe_r2015a#dataaccess).

732 National borders of Mozambique were obtained from <https://gadm.org/data.html>. For the
733 trendline analysis of annual means of maximum wind speeds we use IBTrACS Version 4
734 database, accessible at [https://www.ncei.noaa.gov/data/international-best-track-archive-for-
735 climate-stewardship-ibtracs/v04r00/access/netcdf/IBTrACS.ALL.v04r00.nc](https://www.ncei.noaa.gov/data/international-best-track-archive-for-climate-stewardship-ibtracs/v04r00/access/netcdf/IBTrACS.ALL.v04r00.nc).

736
737 All data used for the figures are publicly available. Maps were generated with QGIS, which
738 can be downloaded at <https://www.qgis.org/>. Satellite imagery background by © Google Maps
739 can be accessed via <http://mt0.google.com/vt/lyrs=s&hl=en&x={x}&y={y}&z={z}>. We used
740 IBTrACS Version 4 to extract the trajectory data of tropical cyclone Idai, available at
741 <https://www.ncei.noaa.gov/products/international-best-track-archive?name=ib-v4-access>.

742 Mozambique admin level 4 shapefiles for Beira are available at
743 [https://data.humdata.org/dataset/mozambique-admin-level-4-beira-and-dondo-
744 neighbourhoud-boundaries](https://data.humdata.org/dataset/mozambique-admin-level-4-beira-and-dondo-neighbourhood-boundaries). GSHHG shoreline data can be accessed via
745 <https://www.ngdc.noaa.gov/mgg/shorelines/data/gshhg/latest/>.

746 Author contributions

747 B.M. and J.S. designed the study, with contributions from T.V., C.O., and K.F. T.V. designed
748 and performed coastal flood model calculations. S.B. estimated flood depths from satellite
749 imagery. B.M. computed the number of affected people and displacements. B.M. and J.S.
750 analyzed the results, and C.O. and K.F. contributed to the interpretation. B.M. and J.S. jointly
751 wrote the paper, with contributions from T.V., S.B., and C.O.

752 Competing interests

753 The authors declare no competing interests.

754 Acknowledgments

755 This research received funding from the European Union's Horizon 2020 research and
756 innovation programme under grant agreement No 820712 (RECEIPT).

757 References

758
759 Angéil, O., Perkins-Kirkpatrick, S., Alexander, L.V., Stone, D., Donat, M.G., Wehner, M.,
760 Shiogama, H., Ciavarella, A., Christidis, N., 2016. Comparing regional precipitation
761 and temperature extremes in climate model and reanalysis products. *Weather Clim.*

762 Extrem. 13, 35–43. <https://doi.org/10.1016/j.wace.2016.07.001>

763 Archila Bustos, M.F., Hall, O., Niedomysl, T., Ernstson, U., 2020. A pixel level evaluation of
764 five multitemporal global gridded population datasets: a case study in Sweden,
765 1990–2015. *Popul. Environ.* 42, 255–277. [https://doi.org/10.1007/s11111-020-00360-](https://doi.org/10.1007/s11111-020-00360-8)
766 8

767 Atmospheric and Environmental Research & African Risk Capacity, 2022. Flood depictions:
768 AER AFED v05r01.

769 Beal, L.M., Vialard, J., Roxy, M.K., lead authors, 2019. IndOOS-2: A roadmap to sustained
770 observations of the Indian Ocean for 2020-203 CLIVAR-4/2019, GOOS-237, 206 pp.,
771 218.

772 Bergensia, 2019. Red Cross: 90 Percent of Beira in Mozambique Destroyed by Cyclone Idai.
773 URL: [https://bergensia.com/red-cross-90-percent-of-beira-in-mozambique-destroyed-](https://bergensia.com/red-cross-90-percent-of-beira-in-mozambique-destroyed-by-cyclone-idai/)
774 [by-cyclone-idai/](https://bergensia.com/red-cross-90-percent-of-beira-in-mozambique-destroyed-by-cyclone-idai/).

775 Bernhofen, M.V., Whyman, C., Trigg, M.A., Sleight, P.A., Smith, A.M., Sampson, C.C.,
776 Yamazaki, D., Ward, P.J., Rudari, R., Pappenberger, F., Dottori, F., Salamon, P.,
777 Winsemius, H.C., 2018. A first collective validation of global fluvial flood models for
778 major floods in Nigeria and Mozambique. *Environ. Res. Lett.* 13, 104007.
779 <https://doi.org/10.1088/1748-9326/aae014>

780 Bilskie, M.V., Hagen, S.C., 2018. Defining Flood Zone Transitions in Low-Gradient Coastal
781 Regions. *Geophys. Res. Lett.* 45, 2761–2770. <https://doi.org/10.1002/2018GL077524>

782 Bloemendaal, N., de Moel, H., Martinez, A.B., Muis, S., Haigh, I.D., van der Wiel, K.,
783 Haarsma, R.J., Ward, P.J., Roberts, M.J., Dullaart, J.C.M., Aerts, J.C.J.H., 2022. A
784 globally consistent local-scale assessment of future tropical cyclone risk. *Sci. Adv.* 8,
785 eabm8438. <https://doi.org/10.1126/sciadv.abm8438>

786 Bloemendaal, N., Haigh, I.D., de Moel, H., Muis, S., Haarsma, R.J., Aerts, J.C.J.H., 2020.
787 Generation of a global synthetic tropical cyclone hazard dataset using STORM. *Sci.*
788 *Data* 7, 40. <https://doi.org/10.1038/s41597-020-0381-2>

789 Bloemendaal, N., Moel, H. de, Mol, J.M., Bosma, P.R.M., Polen, A.N., Collins, J.M., 2021.
790 Adequately reflecting the severity of tropical cyclones using the new Tropical Cyclone
791 Severity Scale. *Environ. Res. Lett.* 16, 014048. [https://doi.org/10.1088/1748-](https://doi.org/10.1088/1748-9326/abd131)
792 [9326/abd131](https://doi.org/10.1088/1748-9326/abd131)

793 Blöschl, G., Hall, J., Viglione, A., Perdigão, R.A.P., Parajka, J., Merz, B., Lun, D., Arheimer,
794 B., Aronica, G.T., Bilbashi, A., Boháč, M., Bonacci, O., Borga, M., Čanjevac, I.,
795 Castellarin, A., Chirico, G.B., Claps, P., Frolova, N., Ganora, D., Gorbachova, L., Gül,
796 A., Hannaford, J., Harrigan, S., Kireeva, M., Kiss, A., Kjeldsen, T.R., Kohnová, S.,
797 Koskela, J.J., Ledvinka, O., Macdonald, N., Mavrova-Guirguinova, M., Mediero, L.,
798 Merz, R., Molnar, P., Montanari, A., Murphy, C., Osuch, M., Ovcharuk, V., Radevski,
799 I., Salinas, J.L., Sauquet, E., Šraj, M., Szolgay, J., Volpi, E., Wilson, D., Zaimi, K.,
800 Živković, N., 2019. Changing climate both increases and decreases European river
801 floods. *Nature* 573, 108–111. <https://doi.org/10.1038/s41586-019-1495-6>

802 Bryant, S., McGrath, H., Boudreault, M., 2022. Gridded flood depth estimates from satellite-
803 derived inundations. *Nat. Hazards Earth Syst. Sci.* 22, 1437–1450.
804 <https://doi.org/10.5194/nhess-22-1437-2022>

805 Cattaneo, C., Beine, M., Fröhlich, C.J., Kniveton, D., Martinez-Zaroso, I., Mastrorillo, M.,
806 Millock, K., Pignatelli, E., Schraven, B., 2019. Human Migration in the Era of Climate
807 Change. *Rev. Environ. Econ. Policy* 13, 189–206.
808 <https://doi.org/10.1093/reep/rez008>

809 Chavas, D.R., Lin, N., Dong, W., Lin, Y., 2016. Observed Tropical Cyclone Size Revisited. *J.*
810 *Clim.* 29, 2923–2939. <https://doi.org/10.1175/JCLI-D-15-0731.1>

811 Chen, D., Rojas, M., Samset, B.H., Cobb, K., Diongue Niang, A., Edwards, P., Emori, S.,
812 Faria, S.H., Hawkins, E., Hope, P., Huybrechts, P., Meinshausen, M., Mustafa, S.K.,
813 Plattner, G.-K., Tréguier, A.-M., 2021. Framing, Context, and Methods. In *Climate*
814 *Change 2021: The Physical Science Basis. Contribution of Working Group I to the*
815 *Sixth Assessment Report of the Intergovernmental Panel on Climate*
816 *Change*[Masson-Delmotte, V., P. Zhai, A. Pirani, S.L. Connors, C. Péan, S. Berger,

817 N. Caud, Y. Chen, L. Goldfarb, M.I. Gomis, M. Huang, K. Leitzell, E. Lonnoy, J.B.R.
818 Matthews, T.K. Maycock, T. Waterfield, O. Yelekçi, R. Yu, and B. Zhou (eds.)).
819 Cambridge University Press, Cambridge, United Kingdom and New York, NY, USA,
820 pp. 147–286, doi:10.1017/9781009157896.003.

821 Church, J.A., Clark, P.U., Cazenave, A., Gregory, J.M., Jevrejeva, S., Levermann, A.,
822 Merrifield, M.A., Milne, G.A., Nerem, R.S., Nunn, P.D., Payne, A.J., Pfeffer, W.T.,
823 Stammer, D., Unnikrishnan, A.S., 2013. Sea Level Change. In: Climate Change
824 2013: The Physical Science Basis. Contribution of Working Group I to the Fifth
825 Assessment Report of the Intergovernmental Panel on Climate Change [Stocker,
826 T.F., D. Qin, G.-K. Plattner, M. Tignor, S.K. Allen, J. Boschung, A. Nauels, Y. Xia, V.
827 Bex and P.M. Midgley (eds.)]. Cambridge University Press, Cambridge, United
828 Kingdom and New York, NY, USA, pp. 1137–1216.

829 Church, J.A., White, N.J., 2011. Sea-Level Rise from the Late 19th to the Early 21st Century.
830 *Surv. Geophys.* 32, 585–602. <https://doi.org/10.1007/s10712-011-9119-1>

831 Church, J.A., White, N.J., Coleman, R., Lambeck, K., Mitrovica, J.X., 2004. Estimates of the
832 Regional Distribution of Sea Level Rise over the 1950–2000 Period. *J. Clim.* 17,
833 2609–2625. [https://doi.org/10.1175/1520-0442\(2004\)017<2609:EOTRDO>2.0.CO;2](https://doi.org/10.1175/1520-0442(2004)017<2609:EOTRDO>2.0.CO;2)

834 Cissé, G., McLeman, R., Adams, H., Aldunce, P., Bowen, K., Campbell-Lendrum, D.,
835 Clayton, S., Ebi, K.L., Hess, J., Huang, C., Liu, Q., McGregor, G., Semenza, J.,
836 Tirado, M.C., 2022. Health, Wellbeing, and the Changing Structure of Communities.
837 In: Climate Change 2022: Impacts, Adaptation, and Vulnerability. Contribution of
838 Working Group II to the Sixth Assessment Report of the Intergovernmental Panel on
839 Climate Change [H.-O. Pörtner, D.C. Roberts, M. Tignor, E.S. Poloczanska, K.
840 Mintenbeck, A. Alegría, M. Craig, S. Langsdorf, S. Lösche, V. Möller, A. Okem, B.
841 Rama (eds.)]. Cambridge University Press, Cambridge, UK and New York, NY, USA,
842 pp. 1041-1170, doi:10.1017/9781009325844.009.

843 CMEMS, 2021. Global ocean gridded L4 sea surface heights and derived variables
844 reprocessed (1993-ongoing). E.U. Copernicus Marine Service (CMEMS).
845 Downloaded 2021-08-02.

846 Cohen, S., Brakenridge, G.R., Kettner, A., Bates, B., Nelson, J., McDonald, R., Huang, Y.-F.,
847 Munasinghe, D., Zhang, J., 2018. Estimating Floodwater Depths from Flood
848 Inundation Maps and Topography. *JAWRA J. Am. Water Resour. Assoc.* 54, 847–
849 858. <https://doi.org/10.1111/1752-1688.12609>

850 Custer, R., Nishijima, K., 2015. Flood vulnerability assessment of residential buildings by
851 explicit damage process modelling. *Nat. Hazards* 78, 461–496.
852 <https://doi.org/10.1007/s11069-015-1725-7>

853 Dangendorf Sönke, Marcos Marta, Wöppelmann Guy, Conrad Clinton P., Frederikse
854 Thomas, Riva Riccardo, 2017. Reassessment of 20th century global mean sea level
855 rise. *Proc. Natl. Acad. Sci.* 114, 5946–5951.
856 <https://doi.org/10.1073/pnas.1616007114>

857 Desai, B., Bresch, D.N., Cazabat, C., Hochrainer-Stigler, S., Mechler, R., Ponserre, S.,
858 Schewe, J., 2021. Addressing the human cost in a changing climate. *Science* 372,
859 1284–1287. <https://doi.org/10.1126/science.abh4283>

860 Dullaart, J.C.M., Muis, S., Bloemendaal, N., Chertova, M.V., Couasnon, A., Aerts, J.C.J.H.,
861 2021. Accounting for tropical cyclones more than doubles the global population
862 exposed to low-probability coastal flooding. *Commun. Earth Environ.* 2, 135.
863 <https://doi.org/10.1038/s43247-021-00204-9>

864 Eilander, D., Couasnon, A., Leijnse, T., Ikeuchi, H., Yamazaki, D., Muis, S., Dullaart, J.,
865 Winsemius, H.C., Ward, P.J., 2022. A globally-applicable framework for compound
866 flood hazard modeling. *EGUsphere* 2022, 1–40. [https://doi.org/10.5194/egusphere-](https://doi.org/10.5194/egusphere-2022-149)
867 2022-149

868 Emanuel, K., 2005. Increasing destructiveness of tropical cyclones over the past 30 years.
869 *Nature* 436, 686–688. <https://doi.org/10.1038/nature03906>

870 Emanuel, K., Ravela, S., Vivant, E., Risi, C., 2006. A Statistical Deterministic Approach to
871 Hurricane Risk Assessment. *Bull. Am. Meteorol. Soc.* 87, 299–314.

872 <https://doi.org/10.1175/BAMS-87-3-299>

873 Emanuel, K.A., 2013. Downscaling CMIP5 climate models shows increased tropical cyclone
874 activity over the 21st century. *Proc. Natl. Acad. Sci. U. S. A.* 110, 12219–12224.
875 <https://doi.org/10.1073/pnas.1301293110>

876 Emanuel, K.A., 1987. The dependence of hurricane intensity on climate. *Nature* 326, 483–
877 485. <https://doi.org/10.1038/326483a0>

878 Emerton, R., Cloke, H., Ficchi, A., Hawker, L., de Wit, S., Speight, L., Prudhomme, C.,
879 Rundell, P., West, R., Neal, J., Cuna, J., Harrigan, S., Titley, H., Magnusson, L.,
880 Pappenberger, F., Klingaman, N., Stephens, E., 2020. Emergency flood bulletins for
881 Cyclones Idai and Kenneth: A critical evaluation of the use of global flood forecasts
882 for international humanitarian preparedness and response. *Int. J. Disaster Risk*
883 *Reduct.* 50, 101811. <https://doi.org/10.1016/j.ijdr.2020.101811>

884 Fowler, H.J., Lenderink, G., Prein, A.F., Westra, S., Allan, R.P., Ban, N., Barbero, R., Berg,
885 P., Blenkinsop, S., Do, H.X., Guerreiro, S., Haerter, J.O., Kendon, E.J., Lewis, E.,
886 Schaer, C., Sharma, A., Villarini, G., Wasko, C., Zhang, X., 2021. Anthropogenic
887 intensification of short-duration rainfall extremes. *Nat. Rev. Earth Environ.* 2, 107–
888 122. <https://doi.org/10.1038/s43017-020-00128-6>

889 Fox-Kemper, B., Hewitt, H.T., Xiao, C., Aðalgeirsdóttir, G., Drijfhout, S.S., Edwards, T.L.,
890 Golledge, N.R., Hemer, M., Kopp, R.E., Krinner, G., Mix, A., Notz, D., Nowicki, S.,
891 Nurhati, I.S., Ruiz, L., Sallée, J.-B., Slangen, A.B.A., Yu, Y., 2021. Ocean,
892 Cryosphere and Sea Level Change. In *Climate Change 2021: The Physical Science*
893 *Basis. Contribution of Working Group I to the Sixth Assessment Report of the*
894 *Intergovernmental Panel on Climate Change* [Masson-Delmotte, V., P. Zhai, A.
895 Pirani, S.L. Connors, C. Péan, S. Berger, N. Caud, Y. Chen, L. Goldfarb, M.I. Gomis,
896 M. Huang, K. Leitzell, E. Lonnoy, J.B.R. Matthews, T.K. Maycock, T. Waterfield, O.
897 Yelekçi, R. Yu, and B. Zhou (eds.)]. Cambridge University Press, Cambridge, United
898 Kingdom and New York, NY, USA, pp. 1211–1362.

899 Frame, D.J., Rosier, S.M., Noy, I., Harrington, L.J., Carey-Smith, T., Sparrow, S.N., Stone,
900 D.A., Dean, S.M., 2020a. Climate change attribution and the economic costs of
901 extreme weather events: a study on damages from extreme rainfall and drought.
902 *Clim. Change* 162, 781–797. <https://doi.org/10.1007/s10584-020-02729-y>

903 Frame, D.J., Wehner, M.F., Noy, I., Rosier, S.M., 2020b. The economic costs of Hurricane
904 Harvey attributable to climate change. *Clim. Change* 160, 271–281.
905 <https://doi.org/10.1007/s10584-020-02692-8>

906 GADM, 2018. Database of Global Administrative Areas.

907 Galantowicz, J.F., Picton, J., 2021. Flood Mapping with Passive Microwave Remote
908 Sensing: Current Capabilities and Directions for Future Development, in: *Earth*
909 *Observation for Flood Applications*. Elsevier, p. 28.

910 Garner Andra J., Mann Michael E., Emanuel Kerry A., Kopp Robert E., Lin Ning, Alley
911 Richard B., Horton Benjamin P., DeConto Robert M., Donnelly Jeffrey P., Pollard
912 David, 2017. Impact of climate change on New York City’s coastal flood hazard:
913 Increasing flood heights from the preindustrial to 2300 CE. *Proc. Natl. Acad. Sci.* 114,
914 11861–11866. <https://doi.org/10.1073/pnas.1703568114>

915 Geiger, T., Frieler, K., Bresch, D.N., 2018. A global historical data set of tropical cyclone
916 exposure (TCE-DAT). *Earth Syst. Sci. Data* 10, 185–194.
917 <https://doi.org/10.5194/essd-10-185-2018>

918 Gemenne, F., 2011. Why the numbers don’t add up: A review of estimates and predictions of
919 people displaced by environmental changes. *Glob. Environ. Change, Migration and*
920 *Global Environmental Change – Review of Drivers of Migration* 21, S41–S49.
921 <https://doi.org/10.1016/j.gloenvcha.2011.09.005>

922 Google Maps (a), 2022. Mozambique. Satellite image. URL:
923 <http://mt0.google.com/vt/lyrs=s&hl=en&x={x}&y={y}&z={z}>. Accessed on 2022-04-27.

924 Google Maps (b), 2022. Greater Area of Beira, Mozambique. Satellite image. URL:
925 <http://mt0.google.com/vt/lyrs=s&hl=en&x={x}&y={y}&z={z}>. Accessed on 2022-04-27.

926 Gudmundsson, L., Boulange, J., Do, H.X., Gosling, S.N., Grillakis, M.G., Koutroulis, A.G.,

927 Leonard, M., Liu, J., Müller Schmied, H., Papadimitriou, L., Pokhrel, Y., Seneviratne,
928 S.I., Satoh, Y., Thiery, W., Westra, S., Zhang, X., Zhao, F., 2021. Globally observed
929 trends in mean and extreme river flow attributed to climate change. *Science* 371,
930 1159–1162. <https://doi.org/10.1126/science.aba3996>

931 Guerreiro, S.B., Fowler, H.J., Barbero, R., Westra, S., Lenderink, G., Blenkinsop, S., Lewis,
932 E., Li, X.-F., 2018. Detection of continental-scale intensification of hourly rainfall
933 extremes. *Nat. Clim. Change* 8, 803–807. <https://doi.org/10.1038/s41558-018-0245-3>

934 Guha-Sapir, D., Below, R., Hoyois, P., 2022. EM-DAT: The CRED/OFDA International
935 Disaster Database. Université Catholique de Louvain-Brussels, Belgium.

936 Gulev, S.K., Thorne, P.W., Ahn, J., Dentener, F.J., Domingues, C.M., Gerland, S., Gong, D.,
937 Kaufman, D.S., Nnamchi, H.C., Quaas, J., Rivera, J.A., Sathyendranath, S., Smith,
938 S.L., Trewin, B., von Schuckmann, K., Vose, R.S., 2021. Changing State of the
939 Climate System. In *Climate Change 2021: The Physical Science Basis. Contribution*
940 *of Working Group I to the Sixth Assessment Report of the Intergovernmental Panel*
941 *on Climate Change* [Masson-Delmotte, V., P. Zhai, A. Pirani, S.L. Connors, C. Péan,
942 S. Berger, N. Caud, Y. Chen, L. Goldfarb, M.I. Gomis, M. Huang, K. Leitzell, E.
943 Lonnoy, J.B.R. Matthews, T.K. Maycock, T. Waterfield, O. Yelekçi, R. Yu, and B.
944 Zhou (eds.)]. Cambridge University Press. In Press.

945 Han, W., Meehl, G.A., Rajagopalan, B., Fasullo, J.T., Hu, A., Lin, J., Large, W.G., Wang, J.,
946 Quan, X.-W., Trenary, L.L., Wallcraft, A., Shinoda, T., Yeager, S., 2010. Patterns of
947 Indian Ocean sea-level change in a warming climate. *Nat. Geosci.* 3, 546–550.
948 <https://doi.org/10.1038/ngeo901>

949 Hawker, L., Rougier, J., Neal, J., Bates, P., Archer, L., Yamazaki, D., 2018. Implications of
950 Simulating Global Digital Elevation Models for Flood Inundation Studies. *Water*
951 *Resour. Res.* 54, 7910–7928. <https://doi.org/10.1029/2018WR023279>

952 HDX, 2019. Mozambique admin level 4 - Beira and Dondo neighbourhood boundaries.

953 Holland, G.J., 1980. An Analytic Model of the Wind and Pressure Profiles in Hurricanes.
954 *Mon. Weather Rev.* 108, 1212–1218. [https://doi.org/10.1175/1520-0493\(1980\)108<1212:AAMOTW>2.0.CO;2](https://doi.org/10.1175/1520-0493(1980)108<1212:AAMOTW>2.0.CO;2)

955 Hollinger, M., Sienkevych, O., 2019. The role of local and regional governments in protecting
956 internally displaced persons (IDPs).

957 IDMC, 2022. “IDMC Global Report on Internal Displacement 2022 Displacement Dataset.”
958 <https://www.internal-displacement.org/database/displacement-data>.

959 IDMC, 2019. Unveiling the cost of internal displacement, The ripple effect: economic impacts
960 of internal displacement.

961 Irish, J.L., Sleath, A., Cialone, M.A., Knutson, T.R., Jensen, R.E., 2014. Simulations of
962 Hurricane Katrina (2005) under sea level and climate conditions for 1900. *Clim.*
963 *Change* 122, 635–649. <https://doi.org/10.1007/s10584-013-1011-1>

964 Jongman, B., Winsemius, H.C., Aerts, J.C.J.H., Coughlan de Perez, E., van Aalst, M.K.,
965 Kron, W., Ward, P.J., 2015. Declining vulnerability to river floods and the global
966 benefits of adaptation. *Proc. Natl. Acad. Sci.* 112, E2271–E2280.
967 <https://doi.org/10.1073/pnas.1414439112>

968 Kam, P.M., Aznar-Siguan, G., Schewe, J., Milano, L., Ginnetti, J., Willner, S., McCaughey,
969 J.W., Bresch, D.N., 2021. Global warming and population change both heighten
970 future risk of human displacement due to river floods. *Environ. Res. Lett.* 16, 044026.
971 <https://doi.org/10.1088/1748-9326/abd26c>

972 Knapp, K.R., Kruk, M.C., Levinson, D.H., Diamond, H.J., Neumann, C.J., 2010. The
973 International Best Track Archive for Climate Stewardship (IBTrACS): Unifying
974 Tropical Cyclone Data. *Bulletin of the American Meteorological Society* 91 (3): 363-
975 76.

976 Knutson, T., Camargo, S.J., Chan, J.C.L., Emanuel, K., Ho, C.-H., Kossin, J., Mohapatra,
977 M., Satoh, M., Sugi, M., Walsh, K., Wu, L., 2020. Tropical Cyclones and Climate
978 Change Assessment: Part II: Projected Response to Anthropogenic Warming. *Bull.*
979 *Am. Meteorol. Soc.* 101, E303–E322. <https://doi.org/10.1175/BAMS-D-18-0194.1>

980 Knutson, T., Camargo, S.J., Chan, J.C.L., Emanuel, K., Ho, C.-H., Kossin, J., Mohapatra,
981

982 M., Satoh, M., Sugi, M., Walsh, K., Wu, L., 2019. Tropical Cyclones and Climate
983 Change Assessment: Part I: Detection and Attribution. *Bull. Am. Meteorol. Soc.* 100,
984 1987–2007. <https://doi.org/10.1175/BAMS-D-18-0189.1>

985 Knutson, T.R., Sirutis, J.J., Zhao, M., Tuleya, R.E., Bender, M., Vecchi, G.A., Villarini, G.,
986 Chavas, D., 2015. Global Projections of Intense Tropical Cyclone Activity for the Late
987 Twenty-First Century from Dynamical Downscaling of CMIP5/RCP4.5 Scenarios. *J.*
988 *Clim.* 28, 7203–7224. <https://doi.org/10.1175/JCLI-D-15-0129.1>

989 Knutson, T.R., Tuleya, R.E., 2008. Tropical cyclones and climate change: revisiting recent
990 studies at GFDL, in: Diaz, H.F., Murnane, R.J. (Eds.), *Climate Extremes and Society*.
991 Cambridge University Press, Cambridge, pp. 120–144.
992 <https://doi.org/10.1017/CBO9780511535840.010>

993 Kossin, J.P., Knapp, K.R., Vimont, D.J., Murnane, R.J., Harper, B.A., 2007. A globally
994 consistent reanalysis of hurricane variability and trends. *Geophys. Res. Lett.* 34.
995 <https://doi.org/10.1029/2006GL028836>

996 Kossin, J.P., Olander, T.L., Knapp, K.R., 2013. Trend Analysis with a New Global Record of
997 Tropical Cyclone Intensity. *J. Clim.* 26, 9960–9976. <https://doi.org/10.1175/JCLI-D-13-00262.1>

999 Kulp, S.A., Strauss, B.H., 2021. CoastalDEM v2.1: A high-accuracy and high-resolution
1000 global coastal elevation model trained on ICESat-2 satellite lidar. *Climate Central*
1001 *Scientific Report* 17.

1002 Kulp, S.A., Strauss, B.H., 2018. CoastalDEM: A global coastal digital elevation model
1003 improved from SRTM using a neural network. *Remote Sens. Environ.* 206, 231–239.
1004 <https://doi.org/10.1016/j.rse.2017.12.026>

1005 Lee, J.-Y., Marotzke, J., Bala, G., Cao, L., Corti, S., Dunne, J.P., Engelbrecht, F., Fischer,
1006 E., Fyfe, J.C., Jones, C., Maycock, A., Mutemi, J., Ndiaye, O., Panickal, S., Zhou, T.,
1007 2021. Future Global Climate: Scenario-Based Projections and Near-Term
1008 Information. In *Climate Change 2021: The Physical Science Basis. Contribution of*
1009 *Working Group I to the Sixth Assessment Report of the Intergovernmental Panel on*
1010 *Climate Change* [Masson-Delmotte, V., P. Zhai, A. Pirani, S.L. Connors, C. Péan, S.
1011 Berger, N. Caud, Y. Chen, L. Goldfarb, M.I. Gomis, M. Huang, K. Leitzell, E. Lonnoy,
1012 J.B.R. Matthews, T.K. Maycock, T. Waterfield, O. Yelekçi, R. Yu, and B. Zhou (eds.)].
1013 C. Cambridge University Press, Cambridge, United Kingdom and New York, NY,
1014 USA, pp. 553–672.

1015 Leyk, S., Gaughan, A.E., Adamo, S.B., de Sherbinin, A., Balk, D., Freire, S., Rose, A.,
1016 Stevens, F.R., Blankespoor, B., Frye, C., Comenetz, J., Sorichetta, A., MacManus,
1017 K., Pistolesi, L., Levy, M., Tatem, A.J., Pesaresi, M., 2019. The spatial allocation of
1018 population: a review of large-scale gridded population data products and their fitness
1019 for use. *Earth Syst. Sci. Data* 11, 1385–1409. <https://doi.org/10.5194/essd-11-1385-2019>

1021 Lin, N., Emanuel, K., Oppenheimer, M., Vanmarcke, E., 2012. Physically based assessment
1022 of hurricane surge threat under climate change. *Nat. Clim. Change* 2, 462–467.
1023 <https://doi.org/10.1038/nclimate1389>

1024 Lin, N., Lane, P., Emanuel, K.A., Sullivan, R.M., Donnelly, J.P., 2014. Heightened hurricane
1025 surge risk in northwest Florida revealed from climatological-hydrodynamic modeling
1026 and paleorecord reconstruction. *J. Geophys. Res. Atmospheres* 119, 8606–8623.
1027 <https://doi.org/10.1002/2014JD021584>

1028 Lindsay, J.B., 2014. The Whitebox Geospatial Analysis Tools Project and Open-Access GIS.
1029 *Proc. GIS Res. UK 22nd Annu. Conf. Univ. Glasg.* 16–18.

1030 Luu, L.N., Scussolini, P., Kew, S., Philip, S., Hariadi, M.H., Vautard, R., Van Mai, K., Van Vu,
1031 T., Truong, K.B., Otto, F., van der Schrier, G., van Aalst, M.K., van Oldenborgh, G.J.,
1032 2021. Attribution of typhoon-induced torrential precipitation in Central Vietnam,
1033 October 2020. *Clim. Change* 169, 24. <https://doi.org/10.1007/s10584-021-03261-3>

1034 Lyard, F.H., Allain, D.J., Cancet, M., Carrère, L., Picot, N., 2021. FES2014 global ocean tide
1035 atlas: design and performance. *Ocean Sci.* 17, 615–649. <https://doi.org/10.5194/os-17-615-2021>

1037 Mandli, K.T., Dawson, C.N., 2014. Adaptive mesh refinement for storm surge. *Ocean Model.*
1038 75, 36–50. <https://doi.org/10.1016/j.ocemod.2014.01.002>

1039 McAdam, J., 2022. Evacuations: a form of disaster displacement? *Forced Migr. Rev.* 56–57.

1040 Mengel, M., Treu, S., Lange, S., Frieler, K., 2021. ATTRICI v1.1 – counterfactual climate for
1041 impact attribution. *Geosci. Model Dev.* 14, 5269–5284. [https://doi.org/10.5194/gmd-](https://doi.org/10.5194/gmd-14-5269-2021)
1042 14-5269-2021

1043 Mester, B., Vogt, T., Bryant, S., Otto, C., Frieler, K., Schewe, J., 2022. TC Idai attribution
1044 study - data collection v1.1 (Version v1.1). doi: 10.5281/zenodo.6907855.

1045 Mester, B., Willner, S.N., Frieler, K., Schewe, J., 2021. Evaluation of river flood extent
1046 simulated with multiple global hydrological models and climate forcings. *Environ.*
1047 *Res. Lett.* 16, 094010. <https://doi.org/10.1088/1748-9326/ac188d>

1048 Muis, S., Apecechea, M.I., Dullaart, J., de Lima Rego, J., Madsen, K.S., Su, J., Yan, K.,
1049 Verlaan, M., 2020. A High-Resolution Global Dataset of Extreme Sea Levels, Tides,
1050 and Storm Surges, Including Future Projections. *Front. Mar. Sci.* 7.
1051 <https://doi.org/10.3389/fmars.2020.00263>

1052 Nicholls, R.J., Lincke, D., Hinkel, J., Brown, S., Vafeidis, A.T., Meyssignac, B., Hanson, S.E.,
1053 Merkens, J.-L., Fang, J., 2021. A global analysis of subsidence, relative sea-level
1054 change and coastal flood exposure. *Nat. Clim. Change* 11, 338–342.
1055 <https://doi.org/10.1038/s41558-021-00993-z>

1056 Nott, J., Hayne, M., 2001. High frequency of ‘super-cyclones’ along the Great Barrier Reef
1057 over the past 5,000 years. *Nature* 413, 508–512. <https://doi.org/10.1038/35097055>

1058 OCHA, 2004. Guiding Principles on Internal Displacement.

1059 Oldenborgh, G.J. van, Wiel, K. van der, Sebastian, A., Singh, R., Arrighi, J., Otto, F.,
1060 Haustein, K., Li, S., Vecchi, G., Cullen, H., 2017. Attribution of extreme rainfall from
1061 Hurricane Harvey, August 2017. *Environ. Res. Lett.* 12, 124009.
1062 <https://doi.org/10.1088/1748-9326/aa9ef2>

1063 O’Neill, B., van Aalst, M., Zaiton Ibrahim, Z., Berrang Ford, L., Bhadwal, S., Buhaug, H.,
1064 Diaz, D., Frieler, K., Garschagen, M., Magnan, A., Midgley, G., Mirzabaev, A.,
1065 Thomas, A., Warren, R., 2022. Key Risks Across Sectors and Regions. In: *Climate*
1066 *Change 2022: Impacts, Adaptation, and Vulnerability. Contribution of Working Group*
1067 *II to the Sixth Assessment Report of the Intergovernmental Panel on Climate Change*
1068 *[H.-O. Pörtner, D.C. Roberts, M. Tignor, E.S. Poloczanska, K. Mintenbeck, A.*
1069 *Alegría, M. Craig, S. Langsdorf, S. Löschke, V. Möller, A. Okem, B. Rama (eds.)].*
1070 Cambridge University Press.

1071 Otto, F.E.L., Harrington, L., Schmitt, K., Philip, S., Kew, S., Oldenborgh, G.J. van, Singh, R.,
1072 Kimutai, J., Wolski, P., 2020. Challenges to Understanding Extreme Weather
1073 Changes in Lower Income Countries. *Bull. Am. Meteorol. Soc.* 101, E1851–E1860.
1074 <https://doi.org/10.1175/BAMS-D-19-0317.1>

1075 Patricola, C.M., Wehner, M.F., 2018. Anthropogenic influences on major tropical cyclone
1076 events. *Nature* 563, 339–346. <https://doi.org/10.1038/s41586-018-0673-2>

1077 Pekel, J.-F., Cottam, A., Gorelick, N., Belward, A.S., 2016. High-resolution mapping of global
1078 surface water and its long-term changes. *Nature* 540, 418–422.
1079 <https://doi.org/10.1038/nature20584>

1080 Probst, P., Annunziato, A., 2019. Tropical Cyclone IDAI: analysis of the wind, rainfall and
1081 storm surge impact. Join Research Centre (EUROPEAN COMMISSION). URL:
1082 [https://www.humanitarianresponse.info/sites/www.humanitarianresponse.info/files/do](https://www.humanitarianresponse.info/sites/www.humanitarianresponse.info/files/documents/files/joint_research_centre_analysis_of_wind_rainfall_and_storm_surge_impact_09_april_2019.pdf)
1083 [cuments/files/joint_research_centre_analysis_of_wind_rainfall_and_storm_surge_im](https://www.humanitarianresponse.info/sites/www.humanitarianresponse.info/files/documents/files/joint_research_centre_analysis_of_wind_rainfall_and_storm_surge_impact_09_april_2019.pdf)
1084 [pact_09_april_2019.pdf](https://www.humanitarianresponse.info/sites/www.humanitarianresponse.info/files/documents/files/joint_research_centre_analysis_of_wind_rainfall_and_storm_surge_impact_09_april_2019.pdf).

1085 ReliefWeb, 2019a. Mozambique: Cyclone Idai & Floods Flash Update No. 10, 26 March
1086 2019. URL: [https://reliefweb.int/report/mozambique/mozambique-cyclone-idai-floods-](https://reliefweb.int/report/mozambique/mozambique-cyclone-idai-floods-flash-update-no-10-26-march-2019)
1087 [flash-update-no-10-26-march-2019](https://reliefweb.int/report/mozambique/mozambique-cyclone-idai-floods-flash-update-no-10-26-march-2019). Accessed on 2023-05-15.

1088 ReliefWeb, 2019b. ‘The First City Completely Devastated by Climate Change’ Tries to
1089 Rebuild after Cyclone Idai. URL: [https://reliefweb.int/report/mozambique/first-city-](https://reliefweb.int/report/mozambique/first-city-completely-devastated-climate-change-tries-rebuild-after-cyclone-idai)
1090 [completely-devastated-climate-change-tries-rebuild-after-cyclone-idai](https://reliefweb.int/report/mozambique/first-city-completely-devastated-climate-change-tries-rebuild-after-cyclone-idai).

1091 Resio, D.T., Irish, J.L., 2016. Tropical Cyclone Storm Surge Risk, in: *Handbook of Coastal*

1092 and Ocean Engineering. WORLD SCIENTIFIC, pp. 1405–1422.
1093 https://doi.org/10.1142/9789813204027_0049

1094 Sauer, I.J., Reese, R., Otto, C., Geiger, T., Willner, S.N., Guillod, B.P., Bresch, D.N., Frieler,
1095 K., 2021. Climate signals in river flood damages emerge under sound regional
1096 disaggregation. *Nat. Commun.* 12, 2128. [https://doi.org/10.1038/s41467-021-22153-](https://doi.org/10.1038/s41467-021-22153-9)
1097 9

1098 Scherrer, S.C., Fischer, E.M., Posselt, R., Liniger, M.A., Croci-Maspoli, M., Knutti, R., 2016.
1099 Emerging trends in heavy precipitation and hot temperature extremes in Switzerland.
1100 *J. Geophys. Res. Atmospheres* 121, 2626–2637.
1101 <https://doi.org/10.1002/2015JD024634>

1102 Schiavina, M., Freire, S., MacManus, K., 2019. GHS population grid multitemporal (1975,
1103 1990, 2000, 2015) R2019A. European Commission, Joint Research Centre (JRC).
1104 <https://doi.org/10.2905/42E8BE89-54FF-464E-BE7B-BF9E64DA5218>

1105 Shen, X., Wang, D., Mao, K., Anagnostou, E., Hong, Y., 2019. Inundation Extent Mapping by
1106 Synthetic Aperture Radar: A Review. *Remote Sens.* 11, 879.
1107 <https://doi.org/10.3390/rs11070879>

1108 Shepherd, T.G., 2016. A Common Framework for Approaches to Extreme Event Attribution.
1109 *Curr. Clim. Change Rep.* 2, 28–38. <https://doi.org/10.1007/s40641-016-0033-y>

1110 Shepherd, T.G., Boyd, E., Calel, R.A., Chapman, S.C., Dessai, S., Dima-West, I.M., Fowler,
1111 H.J., James, R., Maraun, D., Martius, O., Senior, C.A., Sobel, A.H., Stainforth, D.A.,
1112 Tett, S.F.B., Trenberth, K.E., van den Hurk, B.J.J.M., Watkins, N.W., Wilby, R.L.,
1113 Zenghelis, D.A., 2018. Storylines: an alternative approach to representing uncertainty
1114 in physical aspects of climate change. *Clim. Change* 151, 555–571.
1115 <https://doi.org/10.1007/s10584-018-2317-9>

1116 Strauss, B.H., Orton, P.M., Bittermann, K., Buchanan, M.K., Gilford, D.M., Kopp, R.E., Kulp,
1117 S., Massey, C., Moel, H. de, Vinogradov, S., 2021. Economic damages from
1118 Hurricane Sandy attributable to sea level rise caused by anthropogenic climate
1119 change. *Nat. Commun.* 12, 2720. <https://doi.org/10.1038/s41467-021-22838-1>

1120 Takayabu, I., Hibino, K., Sasaki, H., Shiogama, H., Mori, N., Shibutani, Y., Takemi, T., 2015.
1121 Climate change effects on the worst-case storm surge: a case study of Typhoon
1122 Haiyan. *Environ. Res. Lett.* 10, 064011. [https://doi.org/10.1088/1748-](https://doi.org/10.1088/1748-9326/10/6/064011)
1123 9326/10/6/064011

1124 The World Bank, 2022. World Development Indicators. Population, total - Mozambique.

1125 Tozer, B., Sandwell, D.T., Smith, W.H.F., Olson, C., Beale, J.R., Wessel, P., 2019. Global
1126 Bathymetry and Topography at 15 Arc Sec: SRTM15+. *Earth Space Sci.* 6, 1847–
1127 1864. <https://doi.org/10.1029/2019EA000658>

1128 Trenberth, K.E., Fasullo, J.T., Shepherd, T.G., 2015. Attribution of climate extreme events.
1129 *Nat. Clim. Change* 5, 725–730. <https://doi.org/10.1038/nclimate2657>

1130 UK Government Office for Science, 2011. Foresight: Migration and Global Environmental
1131 Change (2011). Final Project Report [WWW Document]. GOV.UK. URL
1132 [https://www.gov.uk/government/publications/migration-and-global-environmental-](https://www.gov.uk/government/publications/migration-and-global-environmental-change-future-challenges-and-opportunities)
1133 change-future-challenges-and-opportunities (accessed 1.4.23).

1134 van Berchum, E.C., van Ledden, M., Timmermans, J.S., Kwakkel, J.H., Jonkman, S.N.,
1135 2020. Rapid flood risk screening model for compound flood events in Beira,
1136 Mozambique. *Nat. Hazards Earth Syst. Sci.* 20, 2633–2646.
1137 <https://doi.org/10.5194/nhess-20-2633-2020>

1138 van den Hurk, B.J.J.M., Baldissera Pacchetti, M., Boere, E., Ciullo, A., Coulter, L., Dessai,
1139 S., Ercin, E., Goulart, H., Hamed, R., Hochrainer-Stigler, S., Koks, E., Kubiczek, P.,
1140 Levermann, A., Mechler, R., van Meersbergen, M., Mester, B., Middelani, R.,
1141 Minderhoud, K., Mysiak, J., Nirandjan, S., van den Oord, G., Otto, C., Sayers, P.,
1142 Schewe, J., Shepherd, T.G., Sillmann, J., Stuparu, D., Vogt, T., Witpas, K., 2023.
1143 Climate impact storylines for assessing socio-economic responses to remote events.
1144 *Clim. Risk Manag.* 100500. <https://doi.org/10.1016/j.crm.2023.100500>

1145 van Oldenborgh, G.J., van der Wiel, K., Kew, S., Philip, S., Otto, F., Vautard, R., King, A.,
1146 Lott, F., Arrighi, J., Singh, R., van Aalst, M., 2021. Pathways and pitfalls in extreme

1147 event attribution. *Clim. Change* 166, 13. <https://doi.org/10.1007/s10584-021-03071-7>
1148 Vogt, T., Treu, S., Mengel, M., Frieler, K., Otto, C., 2022. Assessing the scope and
1149 limitations of a fully-open global TC surge model. Manuscript in preparation.
1150 Warren, M., 2019. Why Cyclone Idai is one of the Southern Hemisphere's most devastating
1151 storms. *Nature*. <https://doi.org/10.1038/d41586-019-00981-6>
1152 Webster, P.J., Holland, G.J., Curry, J.A., Chang, H.-R., 2005. Changes in Tropical Cyclone
1153 Number, Duration, and Intensity in a Warming Environment. *Science* 309, 1844–
1154 1846. <https://doi.org/10.1126/science.1116448>
1155 Wessel, P., Smith, W., 1996. A global, self-consistent, hierarchical, high-resolution shoreline
1156 database. *J. Geophys. Res.* 101, 8741–8743. <https://doi.org/10.1029/96JB00104>
1157 Wulder, M.A., White, J.C., Loveland, T.R., Woodcock, C.E., Belward, A.S., Cohen, W.B.,
1158 Fosnight, E.A., Shaw, J., Masek, J.G., Roy, D.P., 2016. The global Landsat archive:
1159 Status, consolidation, and direction. *Remote Sens. Environ.* 185, 271–283.
1160 Yamazaki, D., Ikeshima, D., Sosa, J., Bates, P.D., Allen, G.H., Pavelsky, T.M., 2019. MERIT
1161 Hydro: A High-Resolution Global Hydrography Map Based on Latest Topography
1162 Dataset. *Water Resour. Res.* 55, 5053–5073. <https://doi.org/10.1029/2019WR024873>
1163 Zscheischler, J., Martius, O., Westra, S., Bevacqua, E., Raymond, C., Horton, R.M., van den
1164 Hurk, B., AghaKouchak, A., Jézéquel, A., Mahecha, M.D., Maraun, D., Ramos, A.M.,
1165 Ridder, N.N., Thiery, W., Vignotto, E., 2020. A typology of compound weather and
1166 climate events. *Nat. Rev. Earth Environ.* 1, 333–347. <https://doi.org/10.1038/s43017-020-0060-z>
1167
1168
1169
1170

1171

1172

1173

1174 Supplementary Material

1175

1176 “Human displacements from tropical cyclone Idai attributable 1177 to climate change”

1178

1179 Benedikt Mester ^{1 2}, Thomas Vogt ¹, Seth Bryant ^{2 3}, Christian Otto ¹, Katja Frieler ¹, and
1180 Jacob Schewe ¹

1181

1182 ¹ Potsdam Institute for Climate Impact Research, Potsdam, Germany

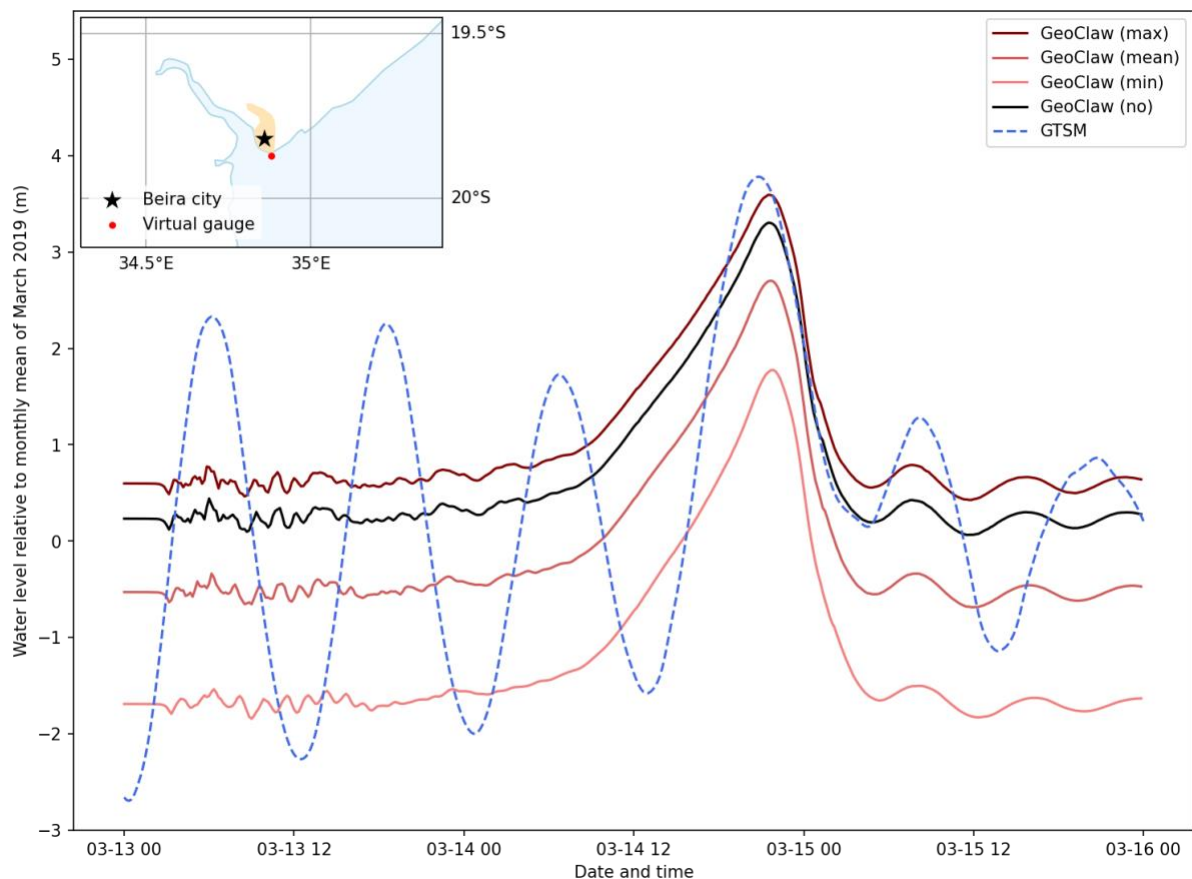
1183 ² Institute of Environmental Science and Geography, Potsdam University, Potsdam,
1184 Germany

1185 ³ GFZ German Research Centre for Geosciences, Potsdam, Germany

1186

1187 Correspondence: Benedikt Mester (benedikt.mester@pik-potsdam.de)

1188

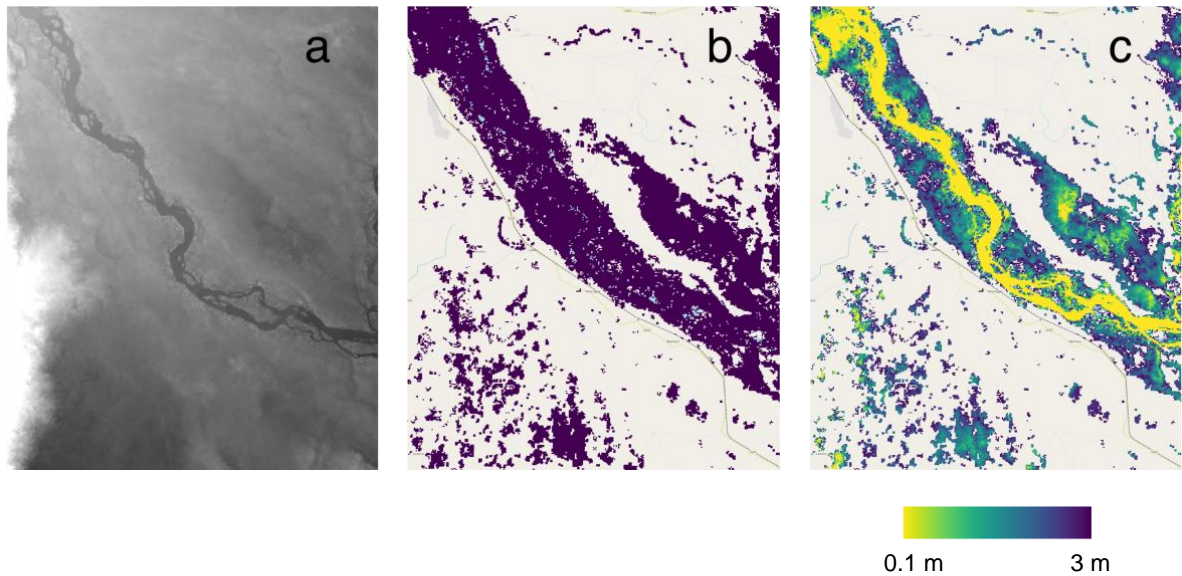


1189

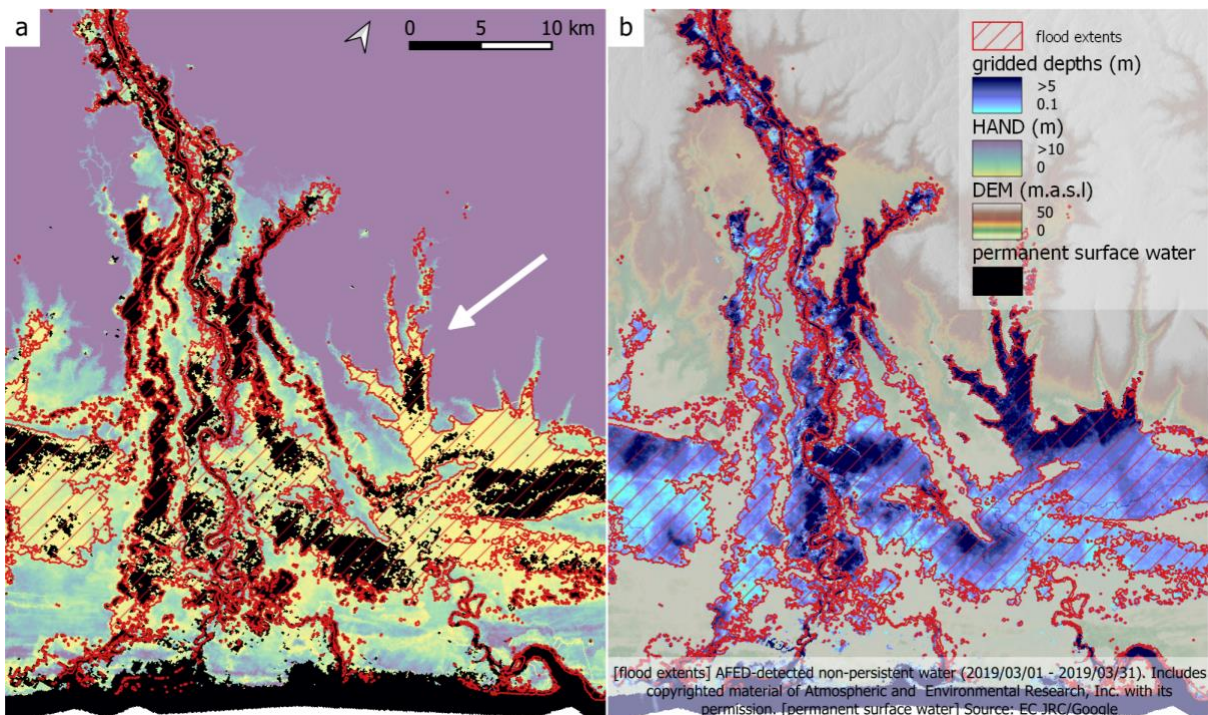
1190 **Figure S1: Water levels at a virtual tide gauge station off the coast of Beira,**
1191 **Mozambique, according to simulations.** Several runs of GeoClaw are compared to GTSM:

1192 The GeoClaw runs are initialized with different base sea levels corresponding to assumptions
1193 of low (min), average (mean), and high (max) astronomical tides at landfall. Another run of
1194 GeoClaw is initialized with the monthly mean sea level from satellite altimetry (no). GTSM is
1195 driven by astronomical tidal forcing, and ERA5 meteorological forcing overlaid by a

1196 parametric TC wind field. While GeoClaw does not incorporate tidal dynamics, the maximum
 1197 surge heights agree well with GTSM.
 1198
 1199



1200
 1201 **Figure S2: Extract of a) MERIT DEM (Yamazaki et al., 2019), b) flood extents obtained**
 1202 **from FloodScan (Atmospheric and Environmental Research & African Risk Capacity**
 1203 **2022), and c) corresponding gridded-depths computed with the RICorDE algorithm.**
 1204 **AFED-detected non-persistent water (2019/03/01 - 2019/03/31). Includes copyrighted material**
 1205 **of Atmospheric and Environmental Research, Inc. with its permission.**
 1206
 1207
 1208

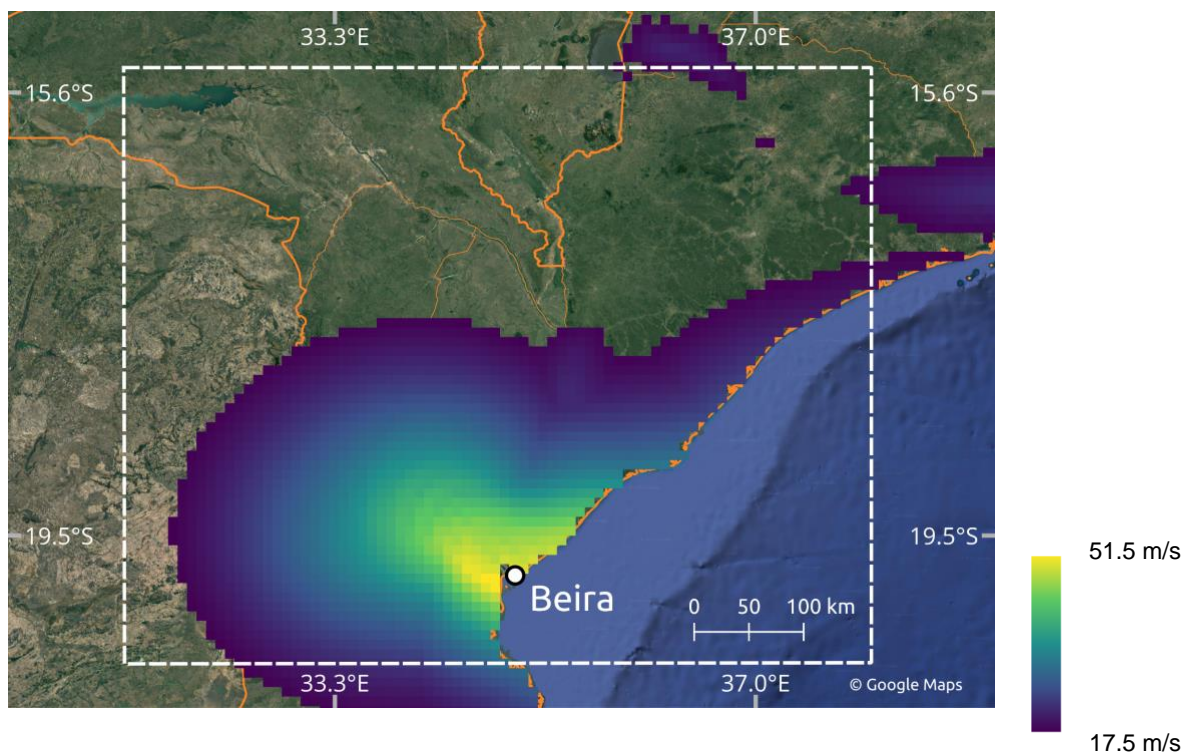


1209

1210 Table S1: Critical flood depths for which the simulated affected people approximately equals
 1211 the 478,000 reported displacements. The closest upper and lower 10 cm flood depth steps
 1212 are shown for each tide.
 1213

Tide	Critical Flood Depth [cm]	Affected People
no	401-410	480,838
no	411-420	474,140
max	391-400	495,714
max	401-410	471,209
min	391-400	495,674
min	401-410	471,148
mean	391-400	502,572
mean	401-410	478,067

1214
 1215 **Figure S3: Example of RICorDE performance against flood extents obtained from**
 1216 **FloodScan (Atmospheric and Environmental Research & African Risk Capacity 2022)**
 1217 **showing a) permanent surface water (Pekel et al., 2016) and resulting HAND values; and**
 1218 **b) MERIT DEM (Yamazaki et al., 2019) and resulting depths values.**
 1219



1220 **Figure S4: Maximum wind speeds of TC Idai, which made landfall in Mozambique in**
 1221 **2019.** White dashed box shows the area of interest in which high wind speed exposure is
 1222 computed; satellite image background by © Google Maps (Google Maps (b), 2022).
 1223

1224

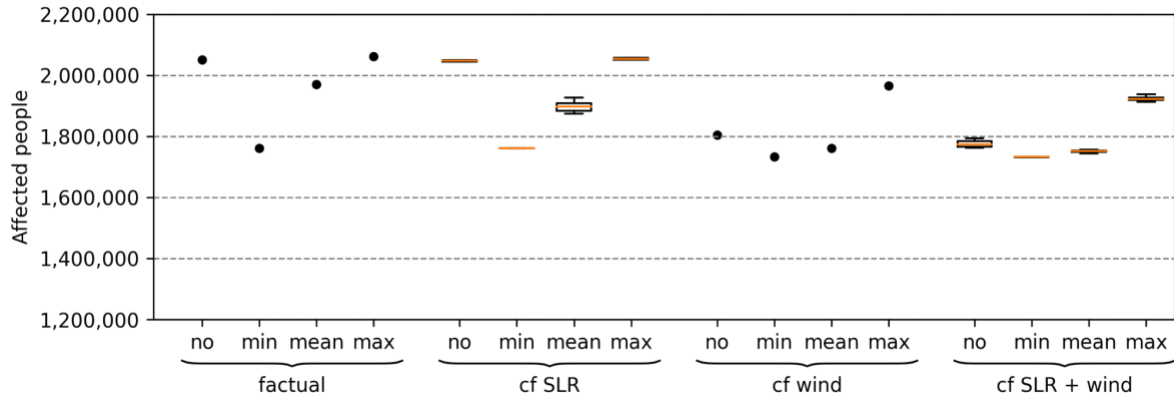
1225 Table S2: Overview main results for modeled affected people. Min./Median/Max. are related
 1226 to the SLR scenarios. Orange background of the first results row indicates the primary
 1227 parameter estimate. Cells with gray background indicate the altered parameter in comparison
 1228 with the primary estimate.
 1229

Counterfactual	Flood Depth Threshold [cm]	Intensification [%]	Tide	Affected Dif.. Min.	Affected Dif.. Median	Affected Dif.. Max	Affected Dif. Min. [%]	Affected Dif. Median [%]	Affected Dif. Max [%]
SLR + wind	100	10	max	35229	36887	39311	2.9	3.0	3.2
SLR + wind	100	10	no	32886	33200	38121	2.7	2.7	3.2
SLR + wind	100	10	min	22557	22557	23481	1.9	1.9	2.0
SLR + wind	100	10	mean	26222	27012	29087	2.2	2.3	2.4
SLR + wind	50	10	max	161895	171054	181243	10.8	11.5	12.3
SLR + wind	10	10	max	123102	138884	148528	6.4	7.2	7.8
SLR	100	10	max	6360	14757	15805	0.5	1.2	1.3
wind	100	10	max	-	24934	-	-	2.6	-
SLR + wind	100	8.5	max	27443	35291	37847	2.2	2.9	3.1
SLR + wind	100	12	max	37784	44583	48181	3.1	3.7	4.0

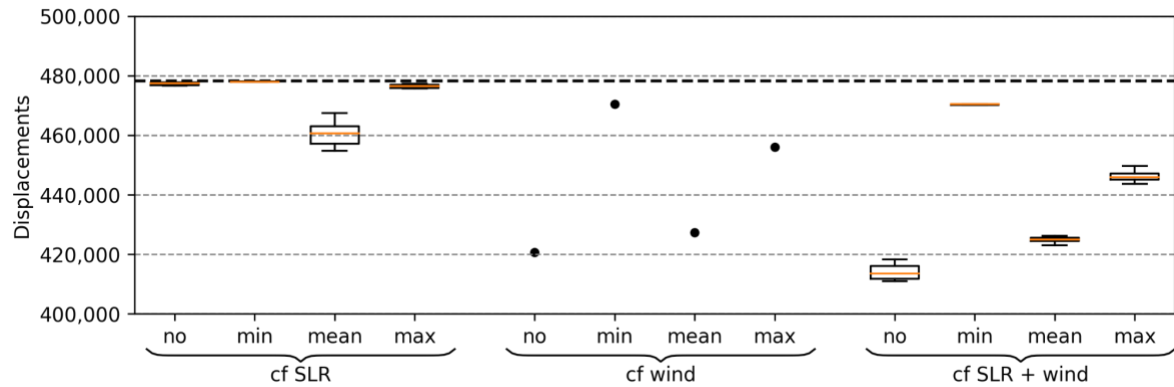
1230

1231

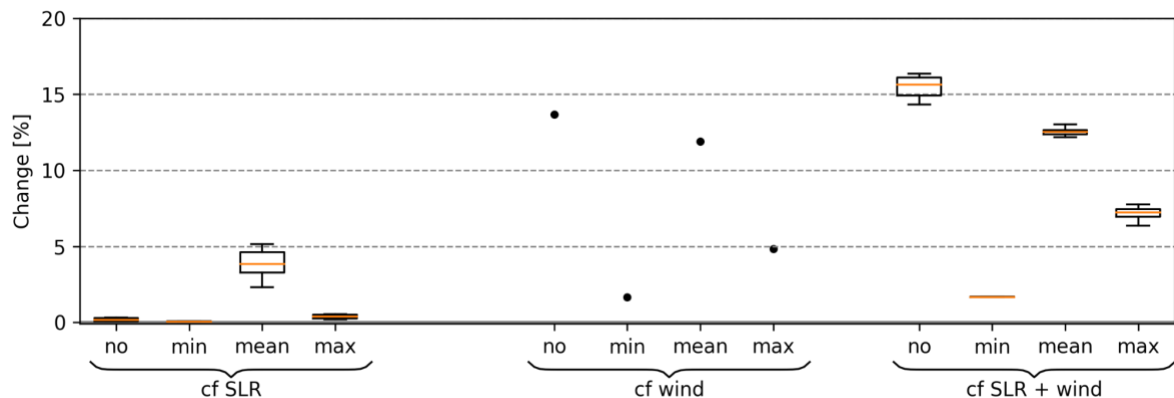
1232
 1233
 1234
 1235
 1236



1237



1238



1239
 1240
 1241
 1242
 1243
 1244
 1245
 1246
 1247
 1248

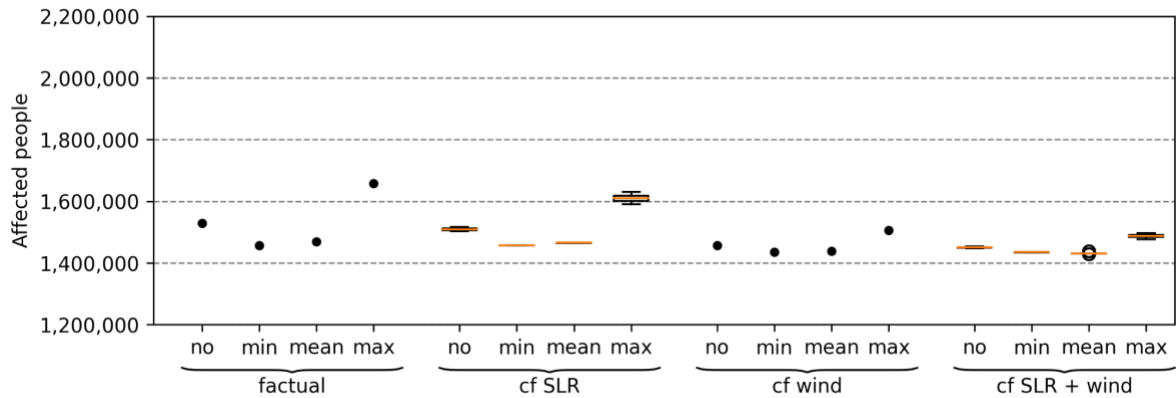
Figure S5: Simulated affected people, displacements and percentage change by flooding (10 cm impact threshold). The percentage change compares factual and counterfactual displacements, and represents the absolute relative change based on the counterfactual results. Three counterfactual scenarios are shown: lower sea level (“cf SLR”), intensification (“cf wind”), and a combination of both (“cf SLR + wind”). Additionally, a variety of counterfactual sea levels as well as a set of astronomical tides is presented, covering minimum (“min”), mean (“mean”), and maximum (“max”) as well as monthly mean sea level from satellite altimetry (“no”). Bold dashed line in the middle panel shows the number of observed displacements. Percentile changes in affected people and displacements are the

1249 same. The second quartile Q2 (median) of the box plot is shown in orange, “whiskers” are
 1250 placed at $\pm 1.5 \cdot$ interquartile range (Q3-Q1).
 1251
 1252

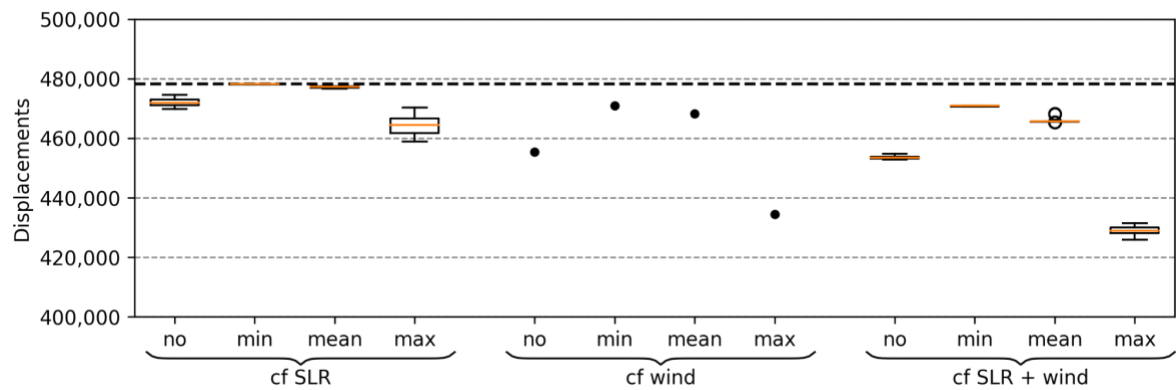
1253

1254

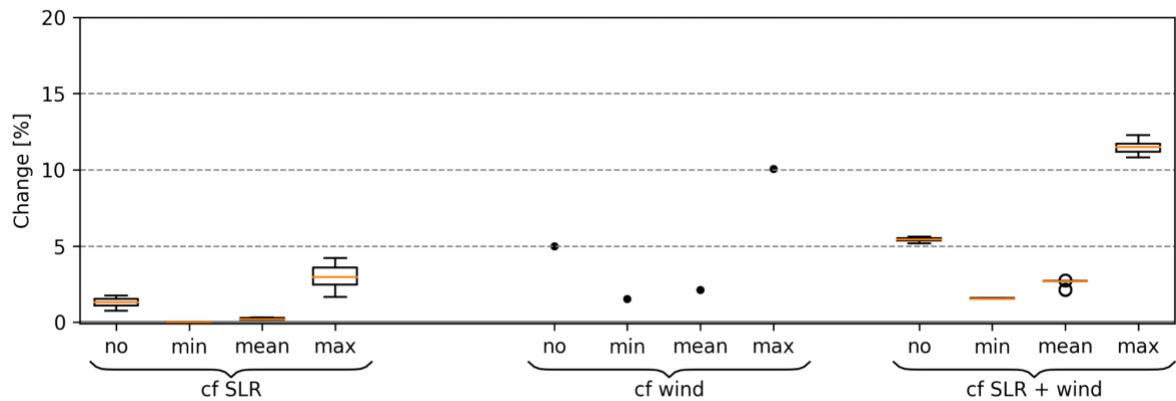
1255



1256



1257



1258

1259 **Figure S6: Simulated affected people, displacements and percentige change by**
 1260 **flooding (50 cm impact threshold).** The percentage change compares factual and
 1261 counterfactual displacements, and represents the absolute relative change based on the
 1262 counterfactual results. Three counterfactual scenarios are shown: lower sea level (“cf
 1263 SLR”), intensification (“cf wind”), and a combination of both (“cf SLR + wind”). Additionally, a

1264 variety of counterfactual sea levels as well as a set of astronomical tides is presented,
1265 covering minimum (“min”), mean (“mean”), and maximum (“max”) as well as monthly mean
1266 sea level from satellite altimetry (“no”). Bold dashed line in the middle panel shows the
1267 number of observed displacements. Percentile changes in affected people and
1268 displacements are the same. The second quartile Q2 (median) of the box plot is shown in
1269 orange, “whiskers” are placed at ± 1.5 * interquartile range (Q3-Q1).

1270
1271
1272

1273
1274
1275
1276
1277
1278
1279